Dynamic Mixture of Progressive Parameter-Efficient Expert Library for Lifelong Robot Learning

Yuheng Lei[1,2], **Sitong Mao**[3], **Shunbo Zhou**[3], **Hongyuan Zhang**[1,2], **Xuelong Li**[2], **Ping Luo**[1,4]
[1] *The University of Hong Kong*
[2] *Institute of Artificial Intelligence (TeleAI), China Telecom*
[3] *Huawei Cloud Computing Technologies*
[4] *HKU Shanghai Intelligent Computing Research Center*
leiyh@connect.hku.hk, pluo@cs.hku.hk

Reviewed on OpenReview: *https://openreview.net/forum?id=MHVBrjS8cG*

Abstract

A generalist agent must continuously learn and adapt throughout its lifetime, achieving efficient forward transfer while minimizing catastrophic forgetting. Previous work within the dominant pretrain-then-finetune paradigm has explored parameter-efficient fine-tuning for single-task adaptation, effectively steering a frozen pretrained model with a small number of parameters. However, in the context of lifelong learning, these methods rely on the impractical assumption of a test-time task identifier and restrict knowledge sharing among isolated adapters. To address these limitations, we propose Dynamic Mixture of Progressive Parameter-Efficient Expert Library (DMPEL) for lifelong robot learning. DMPEL progressively builds a low-rank expert library and employs a lightweight router to dynamically combine experts into an end-to-end policy, enabling flexible and efficient lifelong forward transfer. Furthermore, by leveraging the modular structure of the fine-tuned parameters, we introduce expert coefficient replay, which guides the router to accurately retrieve frozen experts for previously encountered tasks. This technique mitigates forgetting while being significantly more storage- and computation-efficient than experience replay over the entire policy. Extensive experiments on the lifelong robot learning benchmark LIBERO demonstrate that our framework outperforms state-of-the-art lifelong learning methods in success rates during continual adaptation, while utilizing minimal trainable parameters and storage.

1 Introduction

A generalist agent should have the capability to learn and adapt continuously throughout its lifetime, usually termed as *lifelong learning* (De Lange et al., 2021; Masana et al., 2022; Mendez & Eaton, 2023; Wang et al., 2024a). The longstanding challenges are enabling *forward transfer* (i.e., leveraging knowledge from previous tasks to quickly adapt to new ones) and avoiding *catastrophic forgetting* (i.e., retaining previously acquired knowledge when learning new tasks) under *limited computational and memory capacity*.

Due to the notorious sample inefficiency of the traditional *tabula rasa* approach in robotics, researchers have recently explored the *pretrain-then-finetune* paradigm (Brohan et al., 2022; 2023; Kim et al., 2025; Black et al., 2024) that originates from the vision and language domains (Bommasani et al., 2021; Oquab et al., 2024; Radford et al., 2021; Brown et al., 2020). Specifically, this paradigm first pretrain a policy, often referred to as a *vision-language-action* (VLA) model, on large-scale datasets, and then fine-tune it for various downstream tasks.

However, in the context of lifelong learning, naively applying full fine-tuning to sequentially arriving robotic tasks can result in severe forgetting and suboptimal performance, failing to meet our requirements. As depicted in Figure 1, prior work in lifelong robot learning can be broadly classified into three distinct approaches. *Replay* methods (Brohan et al., 2023; Lopez-Paz & Ranzato, 2017; Chaudhry et al., 2019; Shin et al., 2017;

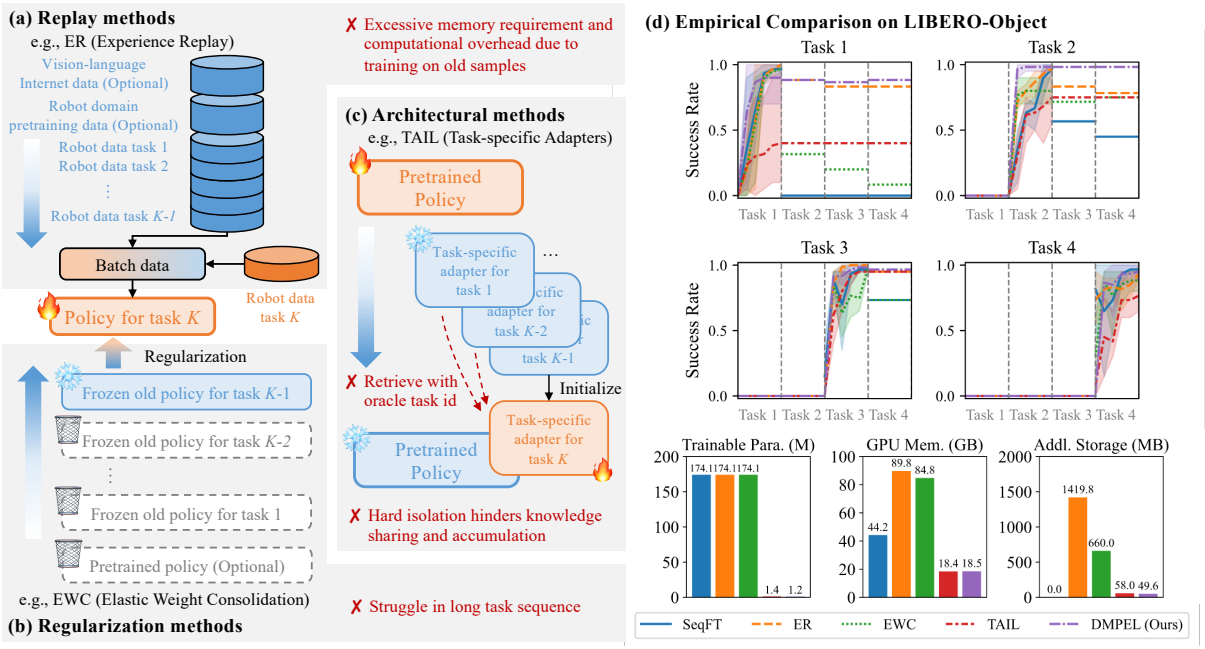

Figure 1: Existing lifelong learning methods: (a) Replay methods; (b) Regularization methods; (c) Architectural methods; (d) Performance on LIBERO-Object. TAIL with LoRA utilizes significantly fewer resources than ER/EWC with FFT and exhibits no forgetting when provided with a task identifier, but demonstrates lower forward transfer. In contrast, DMPEL leverages a low-rank expert library and coefficient replay (CR=5%) to achieve better forward transfer and near-zero forgetting.

Xie & Finn, 2022) retain previous data (e.g., vision-language web data, robot pretraining data, and data from seen tasks) and mix it with in-distribution data during training on new tasks. These methods leads to generalizable policies, but also necessitates huge storage space and computational overhead for retaining old samples. *Regularization* methods (Zenke et al., 2017; Kirkpatrick et al., 2017; Li & Hoiem, 2017) balance between new and old tasks by restricting the update of parameters. For example, EWC (Kirkpatrick et al., 2017) require an entire copy of frozen model from the previous task and entail substantial computation in estimating the importance of parameters. In addition, they usually struggle in long task sequence due to plasticity-stability dilemma.

In contrast, *architectural methods* (Rusu et al., 2016; Mallya & Lazebnik, 2018; Mallya et al., 2018; Ge et al., 2024) address catastrophic forgetting by explicitly learning task-specific parameters. The widely adopted *parameter-efficient fine-tuning* (PEFT) techniques (Ding et al., 2023), such as adapters (Houlsby et al., 2019; Chen et al., 2022), low-rank adaptation (LoRA) (Hu et al., 2021), and prompt tuning (Jia et al., 2022; Li & Liang, 2021; Lester et al., 2021), have proven highly effective for steering frozen foundation models by integrating small, learnable modules in single-task adaptation. In the lifelong learning setting, a practical solution, as exemplified by TAIL (Liu et al., 2024b), involves initializing and training task-specific adapters for each task, subsequently freezing them, and retrieving the appropriate adapter based on the oracle task index. Such method allows efficient adaptation with only a small amount of task-specific parameters, but also exhibits certain limitations. First, assuming test-time task identity is known and retrieving adapter in a hard-coded way could be impractical in real scenarios. Second, failing to effectively share knowledge across isolated adapters result in poor forward transfer. Some prior works construct a shared adapter pool and enable automatic timestep-level retrieval by, for example, performing query-key matching to select the one with highest similarity from a pool of adapters (Schmied et al., 2023), or using multifaceted prototypes to represent the cluster center in the state space for each adapter (Lee et al., 2024), but usually suffer from inaccurate retrieval and suboptimal performance.

In this paper, we introduce the Dynamic Mixture of Progressive Parameter-Efficient Expert Library (DMPEL) to address key challenges in lifelong robot learning. As illustrated in Figure 2, DMPEL features two core innovations: (1) it incrementally constructs a library of low-rank experts and employs a lightweight router to dynamically compose these experts into a unified policy based on the current context. This design

allows the agent to flexibly adapt while leveraging all previously acquired parametric knowledge, thereby **enhancing forward transfer**; (2) it uses expert coefficient replay to regularize the router in accurately integrating experts for all previously encountered tasks, exploiting the modularity of fine-tuned parameters to **prevent catastrophic forgetting**. Notably, replaying low-dimensional embeddings and coefficients using the router is significantly more efficient than replaying demonstrations that require the entire policy in terms of storage and computation. Extensive evaluations on the lifelong manipulation benchmark LIBERO (Liu et al., 2024a) demonstrate that our method achieves superior forward transfer with reduced catastrophic forgetting compared to existing baselines, all while requiring minimal trainable parameters and storage.

2 Related Work

Foundation Models for Robotics. The traditional *tabula rasa* paradigm in robotics is widely criticized for its sample inefficiency, prompting researchers to explore the use of foundation models to improve downstream task transfer (Firoozi et al., 2023; Hu et al., 2023). One prominent direction involves transferring general visual representations: some studies directly employ foundation models from other domains as vision encoders (Parisi et al., 2022; Yuan et al., 2022), such as CLIP (Radford et al., 2021) and DINOv2 (Oquab et al., 2024), while others pretrain visual representations on egocentric video datasets (Nair et al., 2023; Majumdar et al., 2024). Another emerging line of research focuses on pretraining large-scale policies on diverse robotic tasks to capture generalizable behavior priors, for example, RT-2 (Brohan et al., 2023), OpenVLA (Kim et al., 2025), and π_0 (Black et al., 2024). However, when adapting these models to downstream tasks, most approaches either rely on the frozen pretrained model (i.e., zero-shot transfer) or require costly full fine-tuning. Some prior work has explored parameter-efficient fine-tuning (PEFT) by integrating task-specific modules into the pretrained vision encoder (Sharma et al., 2023; Marza et al., 2024) or temporal transformer (Liang et al., 2022; Xu et al., 2023; Qiao et al., 2023). Despite these advancements, most existing work still focuses on single-task adaptation, whereas our approach targets lifelong adaptation to a sequence of new tasks.

Lifelong Learning with PEFT. Compared to full fine-tuning, PEFT optimizes only a small amount of inserted parameters while keeping the rest unchanged, which shares conceptual similarities with *architectural methods* in lifelong learning (Ding et al., 2023). Most studies on PEFT-based lifelong learning predominantly utilize prompt-based tuning (Jia et al., 2022; Lester et al., 2021) to adapt frozen pretrained model for tasks such as image classification, e.g., L2P (Wang et al., 2022c), DualPrompt (Wang et al., 2022b), CODA-Prompt (Smith et al., 2023), DAP (Jung et al., 2023), and text classification, e.g., EPI (Wang et al., 2023b), Progressive Prompts (Razdaibiedina et al., 2023). Current research primarily investigates strategies for dynamically selecting or generating instance-specific prompts (Zhou et al., 2024). Recognizing the representational limitations of prompt tuning, subsequent studies have extended to more powerful PEFT techniques, including LAE (Gao et al., 2023), HiDe-PET (Wang et al., 2025), and SKILL (Ge et al., 2024). Despite the success in incremental classification tasks, its application remains largely unexplored in robotics. A few pioneering works employ LoRA (Hu et al., 2021) to store task-specific knowledge, yet diverge in their retrieval mechanisms: TAIL (Liu et al., 2024b) relies on oracle task identifiers, L2M (Schmied et al., 2023) implements query-key matching between the current context and learnable keys, while IsCiL (Lee et al., 2024) establishes multifaceted prototypes through K-means clustering in the state space, with input states retrieving the closest LoRA parameters based on proximity. Our method incrementally constructs a parameter-efficient expert library and learns a lightweight router to dynamically retrieve and combine these experts.

Mixture of Experts (MoE) and Model Fusion. MoE approach involves training multiple specialized models for specific subtasks and has gained significant attention (Fedus et al., 2022; Muqeeth et al., 2024). A key method for combining these experts is parameter ensemble, supported by the linear mode connectivity phenomenon, which shows models converging to a single low-loss basin (Frankle et al., 2020). Task Arithmetic (Ilharco et al., 2023) introduces *task vectors*, representing the difference between fine-tuned and pretrained models, enhancing multi-task model performance when merged. Follow-up work (Yang et al., 2024; Tang et al., 2024) improves this by learning input-conditioned layer-wise fusion coefficients, increasing flexibility and performance. Model fusion techniques also extend naturally to PEFT. The key idea is that low-rank experts trained on different tasks capture complementary knowledge that can be recombined to solve new tasks, motivating a recent line of work focuses on reusing and combining previously learned adapters to enable

more efficient and scalable task adaptation, including LoRAHub (Huang et al., 2024), AdapterFusion (Pfeiffer et al., 2021), and so on (Wu et al., 2023; 2024; Wang et al., 2022a; Zhao et al., 2024; Ge et al., 2025). In robotics, models like MELA (Yang et al., 2020), MoE-Loco (Huang et al., 2025), MORE (Zhao et al., 2025), and SDP (Wang et al., 2024b) create versatile, adaptive behaviors for multiple tasks by fusing expert sets. Our method aims to enhance forward transfer in lifelong robot learning by flexibly fusing previously learned low-rank experts for each sub-module in the policy according to the current context. Besides, we exploit the modularized design by replaying expert coefficient on the router to mitigate catastrophic forgetting.

3 Problem Formulation

3.1 Lifelong Robot Learning

In this paper, we aim to solve language-conditioned vision-based robot manipulation tasks, which can be formulated as a family of finite-horizon Markov Decision Process (MDP) $\mathcal{M} = (\mathcal{S}, \mathcal{A}, \mathcal{P}, \mathcal{H}, \mathcal{T})$ that share a common state space $\mathcal{S}$, action space $\mathcal{A}$, transition dynamics $\mathcal{P} : \mathcal{S} \times \mathcal{A} \to \mathcal{S}$, and the maximum episode length $\mathcal{H}$. Each task is characterized by $\mathcal{T} \triangleq (d_0, l)$, where d_0 is the initial state distribution and $l : \mathcal{S} \to \{0, 1\}$ is a language-specified goal predicate. The ultimate objective of robot learning is to search for a policy π that maximizes the expected success rate in reaching the goal: $\max_\pi J(\pi) = \mathbb{E}_{s_t, a_t \sim \pi, d_0} \left[\sum_{t=1}^{\mathcal{H}} l(s_t) \right]$.

Due to the significant challenge of sparse reward in robot manipulation, we consider a more practical lifelong imitation learning setting (Liu et al., 2024a;b), where a robot sequentially learns over a stream of tasks $\{\mathcal{T}^1, \cdots, \mathcal{T}^K, \cdots, \mathcal{T}^\kappa\}$ given an expert demonstration dataset $\mathcal{D}^K = \{\tau_n^K\}_{n=1}^N$ for each task $\mathcal{T}^K = (d_0^K, l^K)$. Each expert trajectory τ_n^K can be represented as $(o_0, a_0, \cdots, o_\mathcal{H})$, in which observation o_t at each step t includes RGB images and proprioceptive states. Following common pratice in partially observable MDPs, we approximate current state s_t by stacking prior observations, i.e., $s_t = o_{\leq t} = (o_0, \cdots, o_t)$. We perform behavior cloning (Bain & Sammut, 1995) to learn a stochastic policy π_θ by minimizing the negative log-likelihood loss:

$$\min_\theta L(\theta) = -\mathbb{E}_{\tau_n^K \sim \mathcal{D}^K} \left[\sum_{t=0}^{\mathcal{H}-1} \log \pi_\theta \left(a_t | o_{\leq t}, l^K \right) \right]. \tag{1}$$

3.2 Evaluation Metrics

We use four metrics to evaluate the performance of lifelong robot learning, three of them follow prior works (Liu et al., 2024a; Rodríguez et al., 2018): forward transfer (FWT), negative backward transfer (NBT), area under the success rate curve (AUC), along with an additional metric, the final success rate (Final SR). Formally, we evaluate the policy on current task $\mathcal{T}^K$ when reaching a checkpoint $e \in \mathcal{E} = \{0, \cdots, E-1\}$ (i.e., every multiple epochs of training) and we denote the success rate as $S_{K,K,e}$, where the three subscripts refer to the current training task, the evaluated task, and the epoch number. When the training on current task $\mathcal{T}^K$ is completed, we find the earliest checkpoint e_K^* that achieves the best performance and mark it as the final success rate $S_{K,K}$, i.e., $S_{K,K} = S_{K,K,e_K^*} = \max_{e \in \mathcal{E}} S_{K,K,e}$. We only keep the best checkpoint for future training and evaluation as if the agent stops learning after e_K^*, i.e., for all $e \geq e_K^*$, $S_{K,K,e} = S_{K,K}$. This checkpoint e_K^* will be further evaluated on previous tasks $\mathcal{T}^j, j \leq K$, where the success rate is denoted as $S_{K,j}$. Intuitively, higher FWT indicates faster adaptation to new tasks, lower NBT indicates less catastrophic forgetting on old tasks, and higher AUC demonstrates an overall better performance across tasks and a good balance between FWT and NBT. These metrics can be formally defined as:

$$\text{FWT} = \frac{1}{\kappa} \sum_{K=1}^{\kappa} \left[\frac{1}{|\mathcal{E}|} \sum_{e \in \mathcal{E}} S_{K,K,e} \right], \tag{2}$$

$$\text{NBT} = \frac{1}{\kappa} \sum_{K=1}^{\kappa} \left[\frac{1}{\kappa - K} \sum_{l=K+1}^{\kappa} (S_{K,K} - S_{l,K}) \right], \tag{3}$$

$$\text{AUC} = \frac{1}{\kappa} \sum_{K=1}^{\kappa} \left[\frac{1}{\kappa - K + 1} \Big(\frac{1}{|\mathcal{E}|} \sum_{e \in \mathcal{E}} S_{K,K,e} + \sum_{l=K+1}^{\kappa} S_{l,K} \Big) \right], \tag{4}$$

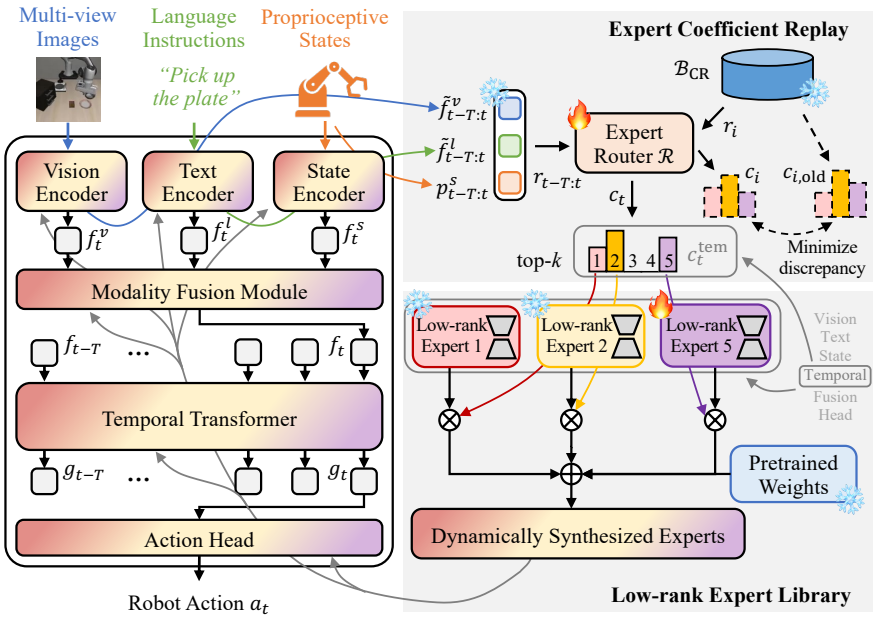

Figure 2: Overview of the proposed method DMPEL.

$$\text{Final SR} = \frac{1}{\kappa} \sum_{K=1}^{\kappa} s_{\kappa,K}. \tag{5}$$

4 Proposed Method

In order to address the key challenges in lifelong robot learning, we propose Dynamic Mixture of Progressive Parameter-Efficient Expert Library (DMPEL). To enhance knowledge transfer, DMPEL incrementally builds a library of low-rank experts and uses a lightweight router to dynamically compose them into a unified policy based on the current context (Section 4.2). To prevent catastrophic forgetting, DMPEL employs expert coefficient replay to regularize the router so it can accurately integrate experts for all previously encountered tasks, leveraging the modularity of fine-tuned parameters (Section 4.3). We provide an overview of DMPEL in Figure 2 and detailed pseudocode in Algorithms 1 (Training) and 2 (Inference, in Appendix).

4.1 Base Policy Architecture

We use a policy similar to the one used in the LIBERO benchmark (Liu et al., 2024a;b) and focus on developing better lifelong learning algorithms. The policy consists of vision, text, and state encoders, an input modality fusion module, a temporal transformer, and an action head.

Vision, text, and state encoders. The policy input is the historical observations $(o_{t-T}, \cdots, o_t)$ and the language instruction $l = \{l_i\}_{i=1}^{L}$, where T is the context length and L is the sentence length. The observation at each step $o_t = (I_t^1, \cdots, I_t^{N_c}, p_t)$ includes RGB images $I_t^{n_c}, 1 \le n_c \le N_c$ from N_c different cameras and low-dimensional proprioceptive states p_t. In experiments, we use images from two cameras, the agent-view image and the eye-in-hand image. We employ the pretrained CLIP ViT-B/16 model (Radford et al., 2021) to serve as the vision encoder $\mathcal{E}_I$ and the text encoder $\mathcal{E}_L$. For the joint states and gripper states, we learn separate linear projection layers $\mathcal{E}_P$ to project the low-dimensional states to proprioceptive embeddings. In summary, at each timestep t, we obtain image embeddings f_t^v, text embeddings f_t^l, and proprioceptive embeddings f_t^s.

Modality fusion. We utilize a feature-wise linear modulation (FiLM) (Perez et al., 2018) to fuse language embeddings with the image and state embeddings. Generally, given the original feature x, the conditional input z, and the fusion network f_{FiLM}, we can obtain the modulated feature $x' = \gamma \odot x + \beta$ where $\gamma, \beta = f_{\text{FiLM}}(z)$.

In our case, the conditional input z refers to the language embedding f_t^l, γ and β are scaling and shifting vectors having the same size as x, and $\odot$ refers to element-wise multiplication.

Temporal transformer and action head. The causal temporal transformer backbone $\mathcal{D}_T$ processes a sequence of multi-modal embeddings to produce a latent vector g_t at each decision-making timestep. We employ a Gaussian Mixture Model (GMM)-based output head $\mathcal{D}_H$ to compute the multi-modal distribution of manipulation actions (Liu et al., 2024b;a). During training, we optimize the negative log-likelihood loss between the action distribution and the ground truth action. At inference time, the robot executes the policy by using the mean of the Gaussian distribution with the highest density for end effectors.

4.2 Low-rank Expert Library

Following the pretrain-then-finetune paradigm, we pretrain the policy on a large-scale robotic dataset and freeze it during the lifelong adaptation to unseen downstream tasks. Low-Rank Adaptation (LoRA) (Hu et al., 2021) is a representative PEFT method that introduces learnable low-rank matrices $\boldsymbol{A} \in \mathbb{R}^{d_{\text{in}} \times r}$, $\boldsymbol{B} \in \mathbb{R}^{r \times d_{\text{out}}}$ and integrate in parallel with the frozen weight matrix $\boldsymbol{W}_0 \in \mathbb{R}^{d_{\text{in}} \times d_{\text{out}}}$ through addition, i.e., $\boldsymbol{W}_0 + \boldsymbol{AB}$. By leveraging the low-rank decomposition $r \ll \min\{d_{\text{in}}, d_{\text{out}}\}$, LoRA substantially reduces the number of trainable parameters. Beyond learning task-specific low-rank adapters that are isolated from one another Liu et al. (2024b), we propose to construct a low-rank expert library on top of the pretrained policy and dynamically reuse low-rank experts from prior tasks, thereby facilitating efficient forward transfer to a new task $\mathcal{T}_k$. While LoRAHub (Huang et al., 2024) and SD-LoRA (Wu et al., 2025) in the vision and language domains share a similar idea of using a task-wise learnable weight vector to combine existing low-rank experts for improved performance on a new task, combination mechanisms to lifelong learning in robotics is even more challenging. First, compared to image or text classification (De Lange et al., 2021; Masana et al., 2022; Wang et al., 2024a) that requires only single forward inference, robotic manipulation is a sequential decision-making process with long horizon. Besides, robot learning requires a mixed types of knowledge, for example, visual concepts, textual task goals, different spatial relationships, and successful adaptation to a new task requires a combination of adaptation in each sub-modules.

Formally, we equip each chosen pretrained linear layer $\mathcal{F} = \{\boldsymbol{W}_0, \boldsymbol{b}_0\}$ with a low-rank expert library $\mathcal{L} = \{\boldsymbol{A}_j, \boldsymbol{B}_j, \boldsymbol{b}_j\}_{j=1}^K$ and use a lightweight router $\mathcal{R}$ to dynamically integrate pretrained and task-specific knowledge based on the current context, providing a more flexible solution for adaptation. Specifically, the router $\mathcal{R} : \mathbb{R}^{d_r} \to \mathbb{R}^{M \times K}$ is implemented as a multi-layer perceptron (MLP) to obtain the dynamic coefficient for each low-rank expert. The router takes the aggregated latent representation $\boldsymbol{r}_{t-T:t} = [\tilde{f}^v_{t-T:t}, \tilde{f}^l_{t-T:t}, p_{t-T:t}] \in \mathbb{R}^{d_r}$ as input, where the subscript $\cdot_{t-T:t}$ indicates mean pooling over the T-step context window. $\tilde{f}^v, \tilde{f}^l$ indicates the visual and text embeddings obtained from the frozen pretrained encoders, distinguishing them from f^v, f^l, which refer to the embeddings that have been modulated by the low-rank experts before being passed to the temporal transformer for action generation. The router input $\boldsymbol{r}_{t-T:t}$ is designed to comprehensively encode the current context while maintaining consistency across lifelong learning stages, which is then transformed into the coefficient vector for low-rank expert activation:

$$\boldsymbol{c}_t = \text{top-}k(\mathcal{R}(\boldsymbol{r}_{t-T:t})) \in \mathbb{R}^{M \times K}. \tag{6}$$

Note that the output $\boldsymbol{c_t}$ is divided into M distinct expert coefficient vectors $\boldsymbol{c}_t^\diamond = [c_{1,t}^\diamond, c_{2,t}^\diamond, \cdots, c_{K,t}^\diamond] \in \mathbb{R}^K$, each assigned to a specific sub-module $\diamond$ in the policy. In our case, we have $M = 6$, consisting of vision encoder, text encoder, state encoder, modality fusion module, temporal transformer, and action head. This design allows each sub-module to use a different coefficient vector to integrate knowledge, providing larger flexibility in adaptation. The top-$k(\cdot)$ operator retains only the top k over K entries of the input vector at their original values, while setting all other coefficients to zero. This ensures efficient utilization of experts by reducing computational overhead while maintaining flexibility for adaptation. Finally, the input-conditioned linear layer $\{\tilde{\boldsymbol{W}}, \tilde{\boldsymbol{b}}\}$ is the dynamic mixture of pretrained weight $\mathcal{F}$ and the low-rank experts from library $\mathcal{L}$:

$$\boldsymbol{y} = \boldsymbol{x}\tilde{\boldsymbol{W}} + \tilde{\boldsymbol{b}} = \underbrace{\boldsymbol{x}\boldsymbol{W}_0 + \boldsymbol{b}_0}_{\text{pretrained}} + \underbrace{\boldsymbol{x} \sum_{j=1}^K c_{j,t} \boldsymbol{A}_j \sum_{j=1}^K c_{j,t} \boldsymbol{B}_j + \sum_{j=1}^K c_{j,t} \boldsymbol{b}_j}_{\text{fine-tuned}}. \tag{7}$$

Algorithm 1 Training Process of DMPEL

Require: Pretrained policy π_θ, router $\mathcal{R}$, low-rank expert library $\mathcal{L} = \varnothing$ for each layer $\mathcal{F}$, coefficient replay buffer $\mathcal{B}_{\text{CR}} = \varnothing$, pruning threshold ξ

for $K = 1, 2, \cdots, \kappa$ **do**
  for each $\{\mathcal{F}, \mathcal{L}\}$ **do**
    Initialize $\boldsymbol{A}_K$, $\boldsymbol{B}_K$, (and optionally $\boldsymbol{b}_K$)
    $\mathcal{L} \leftarrow \text{sg}(\mathcal{L}) \cup \{\boldsymbol{A}_K, \boldsymbol{B}_K, \boldsymbol{b}_K\}$ # $\text{sg}(\cdot)$ means stop gradient, i.e., freezing previously learned experts
  end for
  for epochs $e = 0, 1, 2 \cdots, E-1$ **do**
    $\boldsymbol{c}_{\text{total}} \leftarrow \boldsymbol{0}$
    for each mini-batch data from dataset $\mathcal{D}^K$ **do**
      Compute the context embedding $\boldsymbol{r}$ using the frozen encoders in the pretrained policy π_θ
      Compute the expert coefficient vector $\boldsymbol{c}$ with the router $\mathcal{R}$ using Eq. (6)
      for each $\{\mathcal{F}, \mathcal{L}\}$ **do**
        Obtain the expert coefficient $\boldsymbol{c}^\diamond$ according to which sub-module $\diamond$ the layer belongs to
        Synthesize parameters $\tilde{\boldsymbol{W}}, \tilde{\boldsymbol{b}}$ using Eq. (7)
      end for
      Compute behavior cloning loss L using Eq. (1)
      Update router parameters $\mathcal{R}$ and expert parameters $\boldsymbol{A}_K$, $\boldsymbol{B}_K$, (and optionally $\boldsymbol{b}_K$) to minimize L
      if $e = E - 1$ **then**
        $\mathcal{B}_{\text{CR}} \leftarrow \mathcal{B}_{\text{CR}} \cup \{(\boldsymbol{r}, \boldsymbol{c})\}$ with a probability equals to the coefficient replay ratio
        $\boldsymbol{c}_{\text{total}} \leftarrow \boldsymbol{c}_{\text{total}} + \boldsymbol{c}$
      end if
    end for
  end for
  for epochs $e = 0, 1, 2 \cdots, E-1$ **do**
    for each mini-batch data from the buffer $\mathcal{B}_{\text{CR}}$ **do**
      Compute expert coefficient replay loss L_{CR} using Eq. (8)
      Update router parameters $\mathcal{R}$ to minimize L_{CR}
    end for
  end for
  Delete the LoRA expert from the library and the corresponding output dimension of the router if $\boldsymbol{c}_{\text{total}}[d] \leq \xi, 0 \leq d \leq D-1$ (Optional)
end for

After synthesizing the weights of all layers in the policy, the multi-modal historical observations are converted into robot actions in the manner described in Section 4.1. However, each sub-module within the policy has been dynamically modulated using the low-rank expert library applied on top of the pretrained weights.

During lifelong adaptation, upon the completion of task $\mathcal{T}_k$, we freeze all low-rank experts in the library as acquired knowledge for future retrieval. Then we initialize a new learnable expert for task $\mathcal{T}_{k+1}$. In order to reduce the interference between tasks, we employ the Gram-Schmidt orthogonalization method on $\boldsymbol{A}_{k+1}$ (Smith et al., 2023; Wang et al., 2023a), while other elements $\boldsymbol{B}_{k+1}$ and $\boldsymbol{b}_{k+1}$ are simply zero-initialized. When training on the new task $\mathcal{T}_{k+1}$, the trainable components of the policy include the router $\mathcal{R}$ and the new LoRA experts $\boldsymbol{A}_{k+1}, \boldsymbol{B}_{k+1}, \boldsymbol{b}_{k+1}$. As the LoRA expert library expands, we also simultaneously increases the output dimension of the final linear layer of the router to keep them aligned.

Our design allows the router either to directly reuse previous experts (by assigning zero magnitude on the new expert) or to rely on the new LoRA expert. We empirically investigate this in Section 5.2 on how to control the growing speed of the library and the router by pruning under-activated experts whose coefficients are always close to zero. Formally, at the end of task $\mathcal{T}_k$, we obtain the accumulative expert coefficient $\boldsymbol{c}_{\text{total}}$ and compare each of its dimension with a predefined threshold ξ (we set $\xi = 0.01$ in our experiment). Each coefficient has a one-to-one correspondence with a LoRA expert. If a LoRA expert is deemed underactivated (i.e., $\boldsymbol{c}_{\text{total}}[d] \leq \xi, 0 \leq d \leq D-1$), we prune it from the library and simultaneously remove the corresponding

output dimension of the router. As a result, the size of the LoRA expert library always satisfies $D \leq M \times K$. This pruning mechanism is an optional step within the training loop, as shown in Line 29 of Algorithm 1.

4.3 Expert Coefficient Replay

Although previous LoRA experts are frozen, the router is continuously updated on sequentially arriving tasks. Therefore, incorrect integration of experts, i.e., the expert coefficients under the same context are inaccurate, may also lead to severe catastrophic forgetting and suboptimal performance.

Inspired by replay methods (Chaudhry et al., 2019; Xie & Finn, 2022; Zhao et al., 2024), we propose an expert coefficient replay mechanism that regularizes updates to the lightweight router on previously encountered tasks, thereby mitigating catastrophic forgetting. The implementation involves two phases: (1) During task finalization, we archive a subset of the router's input-output pairs, specifically, the context embedding $\boldsymbol{r}$ and the coefficient vector $\boldsymbol{c}$, in a dedicated buffer $\mathcal{B}_{\text{CR}}$; (2) When adapting to new tasks, we mitigate catastrophic forgetting by enforcing consistency, i.e., requiring the router to generate coefficients that closely match the stored historical coefficients when given the same context. Intuitively, if the router generate parameters $\{\tilde{\boldsymbol{W}}, \tilde{\boldsymbol{b}}\}$ similar to those originally produced during its training on previous tasks, the policy will exhibit consistent behavior. We enforce this by minimizing the mean squared error (MSE) objective between the current and replayed expert activation coefficients:

$$L_{\text{CR}}(\mathcal{R}) = \mathbb{E}_{(\boldsymbol{r}_i, \boldsymbol{c}_{i,\text{old}}) \sim \mathcal{B}_{\text{CR}}} \frac{1}{2} \left(\mathcal{R}(\boldsymbol{r}_i) - \boldsymbol{c}_{i,\text{old}} \right)^2 . \tag{8}$$

With this approach, regardless of the number of tasks encountered, the coefficient vector stored in the buffer can be used to encourage the router to memorize which and how to activate the LoRA expert library on any previously learned task. Compared to conventional experience replay methods that require storing entire trajectories and processing them through the entire policy, our expert coefficient replay strategy leverages the modularity of the low-rank expert library and focuses on regularizing the lightweight router using low-dimensional embeddings and coefficients, resulting in significant reductions in both computational overhead and storage requirements.

5 Experiments

5.1 Experimental Setup

We present an overview of the experimental setup below, with details included in Appendix A.

Benchmark. We conduct extensive evaluation in a lifelong robot learning benchmark LIBERO (Liu et al., 2024a). The robot is situated in a tabletop environment and equipped with a 6-DOF arm and a parallel gripper. We use four lifelong learning task suites: Goal, Spatial, Object, and Long. Each suite consists of 10 sequentially arriving robotic manipulation tasks designed to investigate the transfer of knowledge related to task goals, spatial information, and various objects. The benchmark also includes LIBERO-90, a collection of 90 short-horizon diverse tasks that serves as a pretraining dataset for downstream transfer. All tasks are consistent with the formulation in Section 3, i.e., generating continuous actions to control the robot based on multi-modal input.

Baselines. We consider sequential fine-tuning (SeqFT) baselines (Liu et al., 2024a) that either perform full fine-tuning (FFT) or use frozen pretrained feature (FPF) naively on sequentially arriving tasks. We also consider three representative lifelong learning methods that fine-tune all parameters, including Experience Replay (ER) (Chaudhry et al., 2019), Elastic Weight Consolidation (EWC) (Kirkpatrick et al., 2017), and PackNet (Mallya & Lazebnik, 2018). We also include a hierarchical baseline, LifelOng knowledge Transfer Using Skills (LOTUS) (Wan et al., 2024). Besides, we consider several LoRA-based methods that use different low-rank expert inserting and retrieving mechanism, including Task-specific Adapters for Imitation Learning (TAIL) (Liu et al., 2024b), Learning to Modulate (L2M) (Schmied et al., 2023), and Incremental Learning of Retrievable Skills for Continual Imitation Learning (IsCiL) (Lee et al., 2024). Since TAIL requires oracle

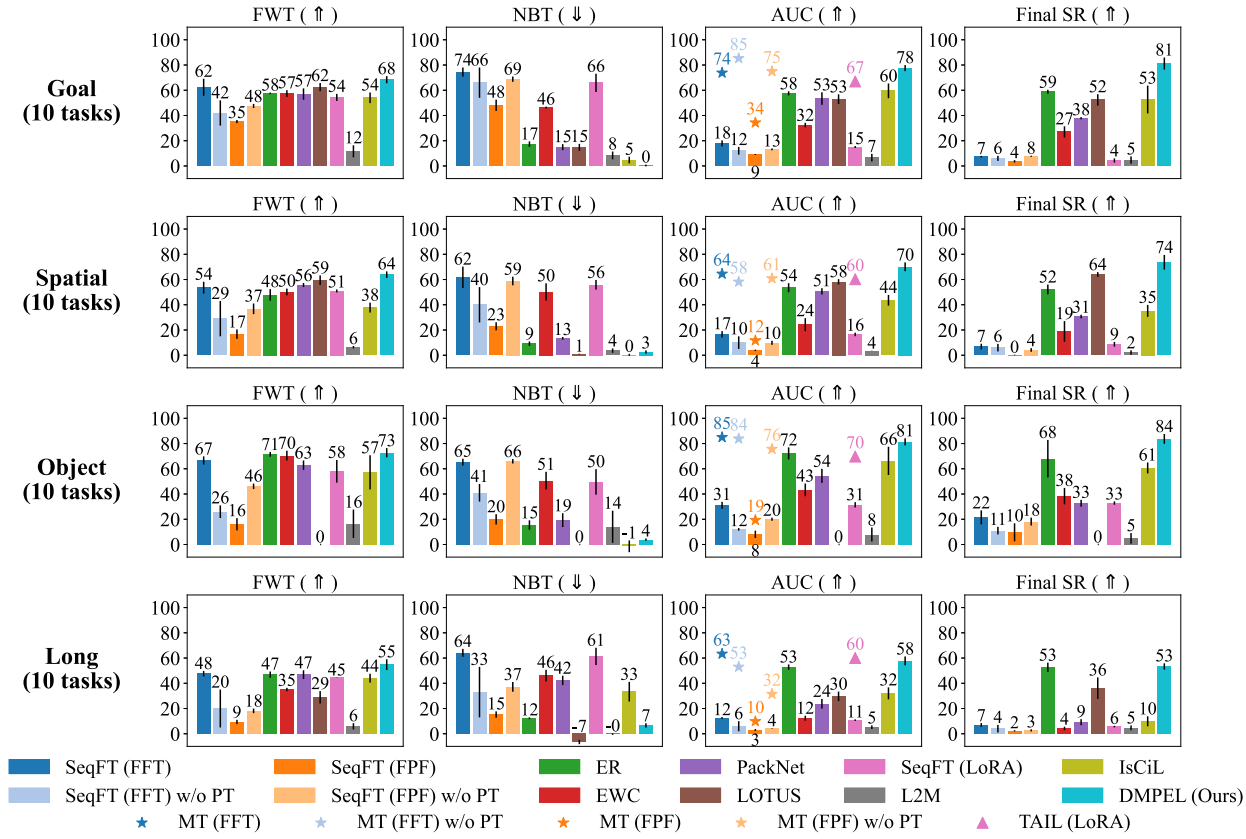

Figure 3: Performance of different lifelong robot learning methods on the LIBERO benchmark.

task identifiers, we also provide the result of SeqFT (LoRA) to align with other methods. Unless otherwise specified, all lifelong methods begin with a policy pretrained (PT) on the LIBERO-90 dataset. We also include the multitask learning (MT) baseline, where the policy leans all tasks simultaneously. Since the AUC metric refers to the area under the success rate curve throughout the learning process, the final success rate of MT is generally regarded as an approximation of the upper bound (albeit not strictly) for any lifelong learning algorithm that are subject to catastrophic forgetting (Liu et al., 2024a).

Implementation Details. We utilize CLIP (Radford et al., 2021) as vision and text encoders, while all other components of the policy is learned from robot demonstrations. The LoRA rank is set to 8 for CLIP encoders and 16 for others, the same as in (Liu et al., 2024b). We pretrain the base policy on the LIBERO-90 dataset and use it as the starting point of lifelong learning. During adaptation, we learn 10 epochs on each arriving task and evaluate every 2 epochs, using a batch size of 32 and AdamW optimizer with a learning rate of 1e-4. We perform expert coefficient replay for 10 epochs after each task. As for the expert router, we employ a scaled sigmoid output activation to restrict the coefficient in [0,2] and use a top-3 strategy to select useful experts. All results are averaged over three random seeds.

5.2 Results and Analysis

Main Results. Figure 4 presents the performance of the pretrained policy on both the original training tasks and zero-shot on unseen tasks, while Figure 3 summarizes three key metrics mentioned in Section 3.2 across all evaluated lifelong learning methods. Pretraining with FFT improves downstream transfer as expected, but still results in poor zero-shot performance, highlighting the need for more effective adaptation strategies. Besides, using frozen CLIP features is inefficient for robotic manipulation and performs even worse when pretraining is applied, likely due to overfitting in other sub-modules. Notably, there is a huge gap between multi-task (MT) and sequential fine-tuning (SeqFT). Among the full fine-tuning methods, ER achieves the best results, but this comes at the cost of storing and replaying large amounts of previous data (see Figure 1). LOTUS fails on the Object suite with the same code as on other suites, indicating poor

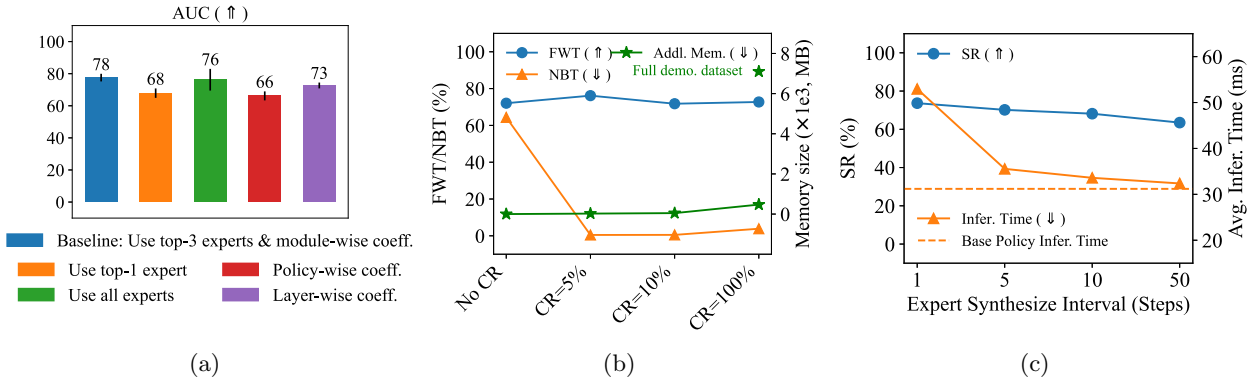

(a) (b) (c)

Figure 5: Ablation studies. (a) Sparse activation of LoRA experts and the granularity of expert coefficients on Goal; (b) Different coefficient replay ratios on Object; (c) Different expert synthesize intervals on Spatial.

robustness. Existing LoRA-based methods show lower forward transfer compared to FFT approaches, while DMPEL improves forward transfer by using dynamically synthesized experts, which reuse previous knowledge in a flexible way. Furthermore, our expert coefficient replay mechanism is highly effective in mitigating catastrophic forgetting, achieving near-zero NBT across all benchmarks without using oracle task identifiers. Conversely, L2M demonstrates weak forward transfer, likely due to its frozen action head. Although IsCiL reduces forgetting on simpler suites, it struggles with long-horizon tasks, presumably because of its fixed context encoding mechanism. In summary, DMPEL achieves efficient forward transfer and low catastrophic forgetting during lifelong learning, with only 1.2M trainable parameters (less than 0.7% of the policy) and minimal storage overhead.

Ablation Studies. In Figure 5a, we conduct an ablation study across two dimensions: the sparse activation of LoRA experts in the library (using top-1 expert, using top-3 experts, and soft merging all experts) and the granularity of expert coefficients (layer-wise, module-wise, and policy-wise). Using top-3 experts yields better performance than using only the top-1 expert and achieves performance comparable to using all experts, demonstrating that appropriate sparsification is beneficial to both the efficiency and performance. Furthermore, assigning distinct coefficients to different submodules enables a more flexible and effective integration of knowledge while preserving simplicity. Figure 5b illustrates the impact of the coefficient replay (CR) ratio on overall performance. CR ratio refers to the proportion of router input-output pairs stored in the buffer for future replay. The results show that coefficient replay does not hinder forward transfer but helps mitigate forgetting efficiently, even when only a small fraction (e.g., 5%) of previous router input-output pairs is retained. Additionally, we demonstrate that replaying the context embeddings and coefficient vectors incurs a much lower storage overhead (approx. 6.7%) compared to replaying full expert demonstrations.

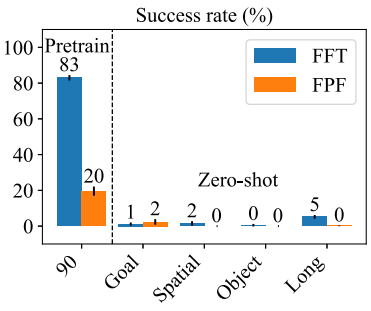

Figure 4: Performance of the pre-trained policy on LIBERO

Computational Overhead. DMPEL introduces two additional stages: (1) encoding the current context with the frozen backbone and using the global router to compute routing coefficients, and (2) averaging the parameters of the top-k experts to synthesize $\tilde{\boldsymbol{W}} \in \mathbb{R}^{d_{\text{in}} \times d_{\text{out}}}$, which incurs approximately $2 \times k \times r \times (d_{\text{in}} + d_{\text{out}})$ FLOPs. The forward pass through the pretrained linear layer requires the usual $2 \times d_{\text{in}} \times d_{\text{out}}$ FLOPs. In robotic manipulation, which typically spans hundreds to thousands of decision steps and whose observations change only gradually from one step to the next. We investigate the influence of the weight synthesis interval (i.e., re-synthesizing policy parameters only every few steps during inference) on the success rate in LIBERO-Spatial, as shown in Figure 5c. The results indicate that the success rate experiences a slight decline as the granularity of the synthesis interval increases. Furthermore, as the synthesis interval expands from 1 to 5, the average inference time quickly approaches that of the backbone-only baseline (approximately 30 ms). This suggests two key points: (1) the expert router dynamically selects low-rank experts tailored to the current context, and less frequent synthesis may result in suboptimal expert coefficients; (2) we can

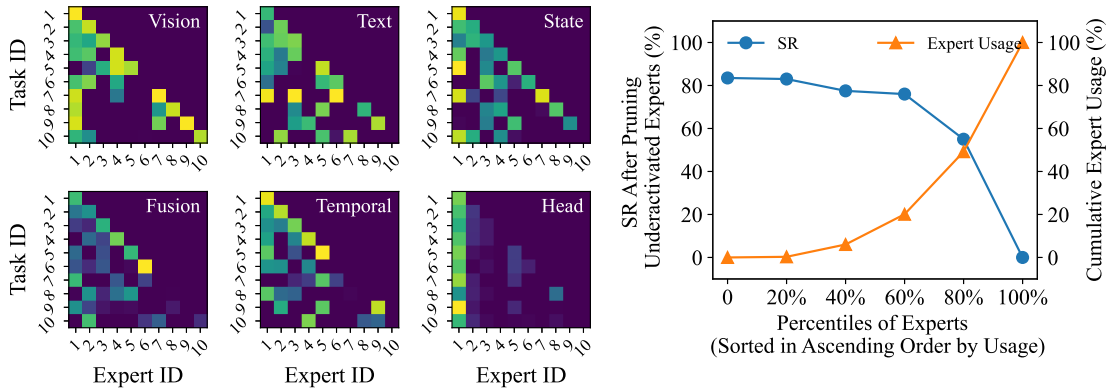

(a) (b)

Figure 6: Analysis on expert coefficients on LIBERO-Object. (a) Visualization of the coefficients for each sub-module in the policy (indicated in the upper right corner), showing to what extent the expert is used by the current task and subsequently reused by later tasks during lifelong adaptation. (b) Influence on the average success rate (SR) when pruning underactivated experts.

achieve a trade-off between the additional computational cost of parameter synthesis and the accuracy of expert coefficients, which directly impacts task performance.

t-SNE Analysis. We present t-SNE visualization in Figure 7, illustrating the latent embeddings from the temporal transformer's final block during the evaluation on Task 2. DMPEL maintains embedding consistency when adapting to new tasks, while other baselines demonstrate significant representation drift and catastrophic forgetting. Results from SeqFT with LoRA indicate that even a small number of parameters can substantially steer the pretrained model, and therefore we should be careful about the forgetting issue during lifelong PEFT. Both DMPEL and EWC impose constraints directly in the parameter space, ensuring consistent representation; however, EWC proves effective only in the short term (after Task 4) and fails to maintain effectiveness in the long run (after Task 8).

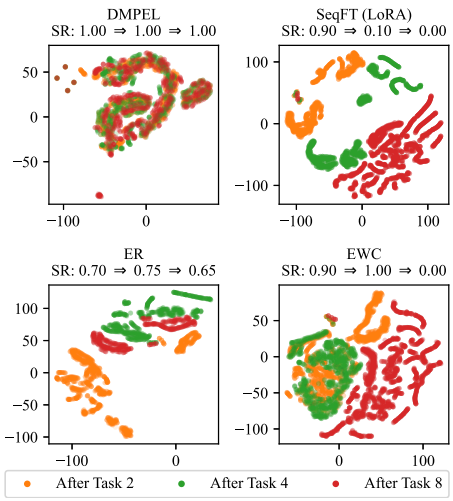

Figure 7: t-SNE visualization of embeddings from the final block when evaluated on Task 2 from LIBERO-Object.

LoRA Expert Activation Analysis. We present a visualization of the expert coefficients for each sub-module during the lifelong learning process on the LIBERO-Object benchmark. As illustrated in Figure 6a, significant knowledge sharing occurs across tasks, which contributes to the enhanced forward transfer capability of DMPEL. Notably, we observe that the low-rank expert learned for the action head in the first task is extensively reused in subsequent tasks, while the experts introduced later are rarely activated. This suggests that these inactive experts can be pruned to further improve storage efficiency without adversely affecting performance, as shown in Figure 6b. We also plot some representative trajectories from different benchmark suites in Figures 8, 14 & 15, with labels indicating the expert ID from the library. In Figure 8, we see that the LoRA expert 4 is actively reused by the vision and state encoder in task 7. Additionally, as the robot executes task 7, we can see the switching process between different experts while approaching, grasping, transporting, and placing down the bowl.

Additional Results. We provide additional results in Appendix B. Section B.1 presents further ablation studies on task order, number of demonstrations, rank size, router design, and top-k mismatch between training and evaluation. Section B.2 highlights the advantages of using a pretrained policy for lifelong learning compared to employing separate small models for each task. Section B.3 offers visualization analysis on

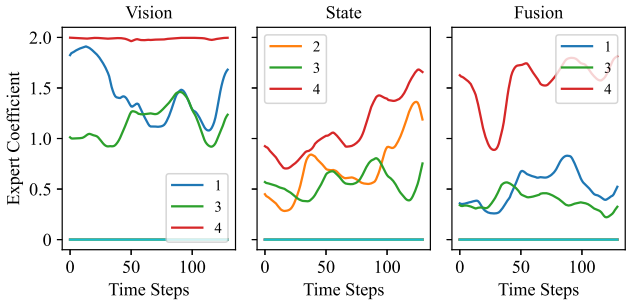

(a) Trajectory of expert coefficient $\boldsymbol{c}$

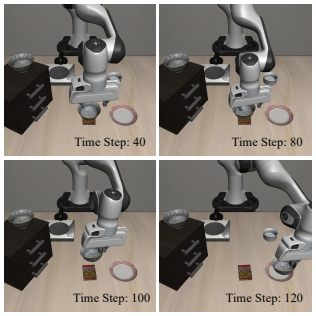

(b) Side-view image

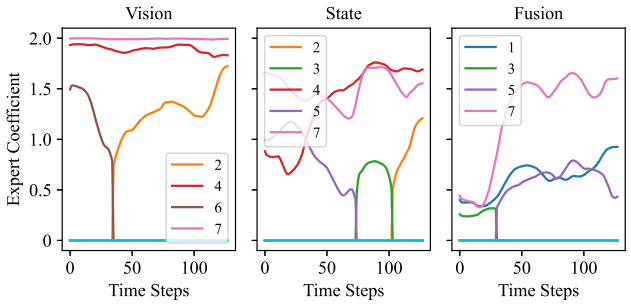

(c) Trajectory of expert coefficient $\boldsymbol{c}$

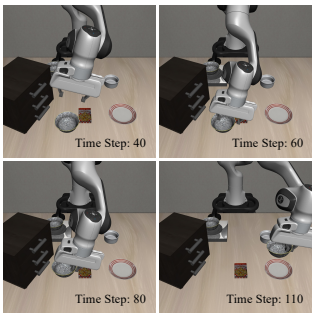

(d) Side-view image

Figure 8: Visualization Analysis on Expert Activation in LIBERO-Spatial: (a)-(b) Task 4: pick up the black bowl on the cookie box and place it on the plate; (c)-(d) Task 7: pick up the black bowl next to the cookie box and place it on the plate.

expert activation trajectories, expert similarities across tasks, and action space coverage. Sections B.4 and B.5 demonstrate the applicability of DMPEL in ultra-long task sequences and cross-domain adaptation, respectively. Finally, Section B.6 presents the learning curves of all methods.

6 Conclusion

We introduce Dynamic Mixture of Progressive Parameter-Efficient Experts Library (DMPEL) for lifelong robot learning. DMPEL incrementally builds a library of low-rank experts and employs a lightweight router to dynamically integrate them, enabling flexible adaptation across diverse scenarios. Leveraging policy modularity, we mitigate catastrophic forgetting via efficient coefficient replay on the router, facilitating expert retrieval without costly experience replay on the entire policy. Our extensive experiments on the LIBERO benchmark show that DMPEL surpasses state-of-the-art lifelong learning baselines in terms of forward transfer and catastrophic forgetting while requiring only very few trainable parameters and storage.

Broader Impact Statement

Despite the improvements, the current work still has several limitations. First, we conducted pretraining and adaptation experiments with a relatively small model, using only simulated data from a single robot. Future work could scale up to larger and more advanced policies (e.g., VLA models with billions of parameters) and investigate transferability to real robots and across different embodiments. In addition, analyzing the mechanisms of knowledge transfer and retention in lifelong learning algorithms could further strengthen the theoretical foundations. Further discussions on limitation and future work is provided in Appendix C. Nonetheless, DMPEL stands as a high-performing and affordable lifelong robot learning framework with great potential in practical applications.

References

Michael Bain and Claude Sammut. A framework for behavioural cloning. In *Machine Intelligence 15*, pp. 103–129, 1995.

Kevin Black, Noah Brown, Danny Driess, Adnan Esmail, Michael Equi, Chelsea Finn, Niccolo Fusai, Lachy Groom, Karol Hausman, Brian Ichter, et al. π_0: A vision-language-action flow model for general robot control. *arXiv preprint arXiv:2410.24164*, 2024.

Rishi Bommasani, Drew A Hudson, Ehsan Adeli, Russ Altman, Simran Arora, Sydney von Arx, Michael S Bernstein, Jeannette Bohg, et al. On the opportunities and risks of foundation models. *arXiv preprint arXiv:2108.07258*, 2021.

Anthony Brohan, Noah Brown, Justice Carbajal, Yevgen Chebotar, Joseph Dabis, et al. RT-1: Robotics transformer for real-world control at scale. *arXiv preprint arXiv:2212.06817*, 2022.

Anthony Brohan, Noah Brown, Justice Carbajal, Yevgen Chebotar, Xi Chen, et al. RT-2: Vision-language-action models transfer web knowledge to robotic control. *arXiv preprint arXiv:2307.15818*, 2023.

Tom Brown, Benjamin Mann, Nick Ryder, Melanie Subbiah, Jared D Kaplan, et al. Language models are few-shot learners. *Advances in Neural Information Processing Systems*, 33:1877–1901, 2020.

Arslan Chaudhry, Marcus Rohrbach, Mohamed Elhoseiny, et al. Continual learning with tiny episodic memories. *arXiv preprint arXiv:1902.10486*, 2019.

Shoufa Chen, Chongjian Ge, Zhan Tong, Jiangliu Wang, Yibing Song, Jue Wang, and Ping Luo. Adaptformer: Adapting vision transformers for scalable visual recognition. *Advances in Neural Information Processing Systems*, 35:16664–16678, 2022.

Cheng Chi, Zhenjia Xu, Siyuan Feng, Eric Cousineau, Yilun Du, Benjamin Burchfiel, Russ Tedrake, and Shuran Song. Diffusion policy: Visuomotor policy learning via action diffusion. *The International Journal of Robotics Research*, 44(10-11):1684–1704, 2025.

Matthias De Lange, Rahaf Aljundi, Marc Masana, Sarah Parisot, Xu Jia, et al. A continual learning survey: Defying forgetting in classification tasks. *IEEE Transactions on Pattern Analysis and Machine Intelligence*, 44(7):3366–3385, 2021.

Ning Ding, Yujia Qin, Guang Yang, Fuchao Wei, Zonghan Yang, et al. Parameter-efficient fine-tuning of large-scale pre-trained language models. *Nature Machine Intelligence*, 5(3):220–235, 2023.

William Fedus, Barret Zoph, and Noam Shazeer. Switch transformers: Scaling to trillion parameter models with simple and efficient sparsity. *Journal of Machine Learning Research*, 23(120):1–39, 2022.

Roya Firoozi, Johnathan Tucker, Stephen Tian, Anirudha Majumdar, Jiankai Sun, Weiyu Liu, et al. Foundation models in robotics: Applications, challenges, and the future. *arXiv preprint arXiv:2312.07843*, 2023.

Jonathan Frankle, Gintare Karolina Dziugaite, Daniel Roy, and Michael Carbin. Linear mode connectivity and the lottery ticket hypothesis. In *International Conference on Machine Learning*, pp. 3259–3269. PMLR, 2020.

Qiankun Gao, Chen Zhao, Yifan Sun, Teng Xi, Gang Zhang, Bernard Ghanem, and Jian Zhang. A unified continual learning framework with general parameter-efficient tuning. In *Proceedings of the IEEE/CVF International Conference on Computer Vision*, pp. 11483–11493, 2023.

Chendi Ge, Xin Wang, Zeyang Zhang, Hong Chen, Jiapei Fan, Longtao Huang, Hui Xue, and Wenwu Zhu. Dynamic mixture of curriculum lora experts for continual multimodal instruction tuning. In *Forty-second International Conference on Machine Learning*, 2025.

Yunhao Ge, Yuecheng Li, Di Wu, Ao Xu, Adam M Jones, Amanda Sofie Rios, Iordanis Fostiropoulos, Po-Hsuan Huang, Zachary William Murdock, Gozde Sahin, et al. Lightweight learner for shared knowledge lifelong learning. *Transactions on Machine Learning Research*, 2024.

Neil Houlsby, Andrei Giurgiu, Stanislaw Jastrzebski, Bruna Morrone, et al. Parameter-efficient transfer learning for nlp. In *International Conference on Machine Learning*, pp. 2790–2799. PMLR, 2019.

Edward J Hu, Phillip Wallis, Zeyuan Allen-Zhu, Yuanzhi Li, Shean Wang, Lu Wang, Weizhu Chen, et al. LoRA: Low-rank adaptation of large language models. In *International Conference on Learning Representations*, 2021.

Yafei Hu, Quanting Xie, Vidhi Jain, Jonathan Francis, Jay Patrikar, Nikhil Keetha, et al. Toward general-purpose robots via foundation models: A survey and meta-analysis. *arXiv preprint arXiv:2312.08782*, 2023.

Chengsong Huang, Qian Liu, Bill Yuchen Lin, Tianyu Pang, Chao Du, and Min Lin. Lorahub: Efficient cross-task generalization via dynamic lora composition. In *First Conference on Language Modeling*, 2024.

Runhan Huang, Shaoting Zhu, Yilun Du, and Hang Zhao. MoE-Loco: Mixture of experts for multitask locomotion. *arXiv preprint arXiv:2503.08564*, 2025.

Gabriel Ilharco, Marco Tulio Ribeiro, Mitchell Wortsman, Ludwig Schmidt, Hannaneh Hajishirzi, and Ali Farhadi. Editing models with task arithmetic. In *The Eleventh International Conference on Learning Representations*, 2023.

Menglin Jia, Luming Tang, Bor-Chun Chen, Claire Cardie, Serge Belongie, Bharath Hariharan, and Ser-Nam Lim. Visual prompt tuning. In *European Conference on Computer Vision*, pp. 709–727. Springer, 2022.

Dahuin Jung, Dongyoon Han, Jihwan Bang, and Hwanjun Song. Generating instance-level prompts for rehearsal-free continual learning. In *Proceedings of the IEEE/CVF International Conference on Computer Vision*, pp. 11847–11857, 2023.

Moo Jin Kim, Karl Pertsch, Siddharth Karamcheti, Ted Xiao, Ashwin Balakrishna, Suraj Nair, Rafael Rafailov, Ethan P Foster, Pannag R Sanketi, Quan Vuong, et al. Openvla: An open-source vision-language-action model. In *8th Annual Conference on Robot Learning*, 2025.

James Kirkpatrick, Razvan Pascanu, Neil Rabinowitz, et al. Overcoming catastrophic forgetting in neural networks. *Proceedings of the National Academy of Sciences*, 114(13):3521–3526, 2017.

Daehee Lee, Minjong Yoo, Woo Kyung Kim, Wonje Choi, and Honguk Woo. Incremental learning of retrievable skills for efficient continual task adaptation. *Advances in Neural Information Processing Systems*, 37:17286–17312, 2024.

Brian Lester, Rami Al-Rfou, and Noah Constant. The power of scale for parameter-efficient prompt tuning. In *Proceedings of the 2021 Conference on Empirical Methods in Natural Language Processing*, pp. 3045–3059, 2021.

Xiang Lisa Li and Percy Liang. Prefix-tuning: Optimizing continuous prompts for generation. In *Proceedings of the 59th Annual Meeting of the Association for Computational Linguistics and the 11th International Joint Conference on Natural Language Processing (Volume 1: Long Papers)*, pp. 4582–4597, 2021.

Zhizhong Li and Derek Hoiem. Learning without forgetting. *IEEE Transactions on Pattern Analysis and Machine Intelligence*, 40(12):2935–2947, 2017.

Anthony Liang, Ishika Singh, Karl Pertsch, and Jesse Thomason. Transformer adapters for robot learning. In *CoRL 2022 Workshop on Pre-training Robot Learning*, 2022.

Bo Liu, Yifeng Zhu, Chongkai Gao, Yihao Feng, Qiang Liu, Yuke Zhu, and Peter Stone. Libero: Benchmarking knowledge transfer for lifelong robot learning. *Advances in Neural Information Processing Systems*, 36, 2024a.

Zuxin Liu, Jesse Zhang, Kavosh Asadi, Yao Liu, et al. TAIL: Task-specific adapters for imitation learning with large pretrained models. In *International Conference on Learning Representations*, 2024b. URL https://openreview.net/forum?id=RRayv1ZPN3.

David Lopez-Paz and Marc'Aurelio Ranzato. Gradient episodic memory for continual learning. *Advances in Neural Information Processing Systems*, 30:6470–6479, 2017.

Arjun Majumdar, Karmesh Yadav, Sergio Arnaud, Jason Ma, et al. Where are we in the search for an artificial visual cortex for embodied intelligence? *Advances in Neural Information Processing Systems*, 36, 2024.

Arun Mallya and Svetlana Lazebnik. Packnet: Adding multiple tasks to a single network by iterative pruning. In *Proceedings of the IEEE Conference on Computer Vision and Pattern Recognition*, pp. 7765–7773, 2018.

Arun Mallya, Dillon Davis, and Svetlana Lazebnik. Piggyback: Adapting a single network to multiple tasks by learning to mask weights. In *European Conference on Computer Vision*, pp. 67–82, 2018.

Ajay Mandlekar, Danfei Xu, Josiah Wong, Soroush Nasiriany, Chen Wang, Rohun Kulkarni, Li Fei-Fei, Silvio Savarese, Yuke Zhu, and Roberto Martín-Martín. What matters in learning from offline human demonstrations for robot manipulation. In *Conference on Robot Learning*, pp. 1678–1690. PMLR, 2022.

Pierre Marza, Laetitia Matignon, Olivier Simonin, and Christian Wolf. Task-conditioned adaptation of visual features in multi-task policy learning. In *Proceedings of the IEEE/CVF Conference on Computer Vision and Pattern Recognition*, pp. 17847–17856, 2024.

Marc Masana, Xialei Liu, Bartłomiej Twardowski, Mikel Menta, et al. Class-incremental learning: survey and performance evaluation on image classification. *IEEE Transactions on Pattern Analysis and Machine Intelligence*, 45(5):5513–5533, 2022.

Jorge A Mendez and Eric Eaton. How to reuse and compose knowledge for a lifetime of tasks: A survey on continual learning and functional composition. *Transactions on Machine Learning Research*, 2023. ISSN 2835-8856. URL https://openreview.net/forum?id=VynY6Bk03b.

Mohammed Muqeeth, Haokun Liu, and Colin Raffel. Soft merging of experts with adaptive routing. *Transactions on Machine Learning Research*, 2024.

Suraj Nair, Aravind Rajeswaran, Vikash Kumar, Chelsea Finn, and Abhinav Gupta. R3M: A universal visual representation for robot manipulation. In *Conference on Robot Learning*, pp. 892–909. PMLR, 2023.

Maxime Oquab, Timothée Darcet, Théo Moutakanni, Huy V. Vo, et al. DINOv2: Learning robust visual features without supervision. *Transactions on Machine Learning Research*, 2024. ISSN 2835-8856. URL https://openreview.net/forum?id=a68SUt6zFt.

Simone Parisi, Aravind Rajeswaran, et al. The unsurprising effectiveness of pre-trained vision models for control. In *International Conference on Machine Learning*, pp. 17359–17371. PMLR, 2022.

Ethan Perez, Florian Strub, Harm De Vries, Vincent Dumoulin, and Aaron Courville. Film: Visual reasoning with a general conditioning layer. In *Proceedings of the AAAI conference on artificial intelligence*, volume 32, 2018.

Jonas Pfeiffer, Aishwarya Kamath, Andreas Rücklé, Kyunghyun Cho, and Iryna Gurevych. Adapterfusion: Non-destructive task composition for transfer learning. In *Proceedings of the 16th Conference of the European Chapter of the Association for Computational Linguistics: Main Volume*, pp. 487–503, 2021.

Yanyuan Qiao, Zheng Yu, and Qi Wu. Vln-petl: Parameter-efficient transfer learning for vision-and-language navigation. In *Proceedings of the IEEE/CVF International Conference on Computer Vision (ICCV)*, pp. 15443–15452, October 2023.

Alec Radford, Jong Wook Kim, Chris Hallacy, et al. Learning transferable visual models from natural language supervision. In *International Conference on Machine Learning*, pp. 8748–8763. PMLR, 2021.

Anastasia Razdaibiedina, Yuning Mao, Rui Hou, Madian Khabsa, Mike Lewis, and Amjad Almahairi. Progressive prompts: Continual learning for language models. In *The Eleventh International Conference on Learning Representations*, 2023.

Natalia Díaz Rodríguez, Vincenzo Lomonaco, David Filliat, and Davide Maltoni. Don't forget, there is more than forgetting: new metrics for continual learning. *arXiv preprint arXiv:1810.13166*, 2018.

Andrei A Rusu, Neil C Rabinowitz, Guillaume Desjardins, Hubert Soyer, James Kirkpatrick, Koray Kavukcuoglu, Razvan Pascanu, and Raia Hadsell. Progressive neural networks. *arXiv preprint arXiv:1606.04671*, 2016.

Thomas Schmied, Markus Hofmarcher, Fabian Paischer, Razvan Pascanu, and Sepp Hochreiter. Learning to modulate pre-trained models in rl. *Advances in Neural Information Processing Systems*, 36, 2023.

Mohit Sharma, Claudio Fantacci, Yuxiang Zhou, et al. Lossless adaptation of pretrained vision models for robotic manipulation. In *International Conference on Learning Representations*, 2023.

Hanul Shin, Jung Kwon Lee, Jaehong Kim, and Jiwon Kim. Continual learning with deep generative replay. *Advances in Neural Information Processing Systems*, 30:2994–3003, 2017.

James Seale Smith, Leonid Karlinsky, Vyshnavi Gutta, et al. Coda-prompt: Continual decomposed attention-based prompting for rehearsal-free continual learning. In *Proceedings of the IEEE/CVF Conference on Computer Vision and Pattern Recognition*, pp. 11909–11919, 2023.

Anke Tang, Li Shen, Yong Luo, Nan Yin, Lefei Zhang, and Dacheng Tao. Merging multi-task models via weight-ensembling mixture of experts. In *Proceedings of the 41st International Conference on Machine Learning*, pp. 47778–47799, 2024.

Weikang Wan, Yifeng Zhu, Rutav Shah, and Yuke Zhu. Lotus: Continual imitation learning for robot manipulation through unsupervised skill discovery. In *2024 IEEE International Conference on Robotics and Automation (ICRA)*, pp. 537–544. IEEE, 2024.

Liyuan Wang, Xingxing Zhang, Hang Su, and Jun Zhu. A comprehensive survey of continual learning: theory, method and application. *IEEE Transactions on Pattern Analysis and Machine Intelligence*, 2024a.

Liyuan Wang, Jingyi Xie, Xingxing Zhang, Hang Su, and Jun Zhu. Hide-pet: continual learning via hierarchical decomposition of parameter-efficient tuning. *IEEE Transactions on Pattern Analysis and Machine Intelligence*, 2025.

Xiao Wang, Tianze Chen, Qiming Ge, Han Xia, Rong Bao, Rui Zheng, Qi Zhang, Tao Gui, and Xuanjing Huang. Orthogonal subspace learning for language model continual learning. In *The 2023 Conference on Empirical Methods in Natural Language Processing*, 2023a.

Yaqing Wang, Sahaj Agarwal, Subhabrata Mukherjee, Xiaodong Liu, Jing Gao, Ahmed Hassan, and Jianfeng Gao. Adamix: Mixture-of-adaptations for parameter-efficient model tuning. In *Proceedings of the 2022 Conference on Empirical Methods in Natural Language Processing*, pp. 5744–5760, 2022a.

Yixiao Wang, Yifei Zhang, Mingxiao Huo, Thomas Tian, Xiang Zhang, Yichen Xie, Chenfeng Xu, Pengliang Ji, Wei Zhan, Mingyu Ding, et al. Sparse diffusion policy: A sparse, reusable, and flexible policy for robot learning. In *8th Annual Conference on Robot Learning*, 2024b.

Zhicheng Wang, Yufang Liu, Tao Ji, Xiaoling Wang, Yuanbin Wu, Congcong Jiang, Ye Chao, Zhencong Han, Ling Wang, Xu Shao, et al. Rehearsal-free continual language learning via efficient parameter isolation. In *Proceedings of the 61st Annual Meeting of the Association for Computational Linguistics (Volume 1: Long Papers)*, pp. 10933–10946, 2023b.

Zifeng Wang, Zizhao Zhang, Sayna Ebrahimi, et al. Dualprompt: Complementary prompting for rehearsal-free continual learning. In *European Conference on Computer Vision*, pp. 631–648. Springer, 2022b.

Zifeng Wang, Zizhao Zhang, Chen-Yu Lee, Han Zhang, et al. Learning to prompt for continual learning. In *Proceedings of the IEEE/CVF Conference on Computer Vision and Pattern Recognition*, pp. 139–149, 2022c.

Chengyue Wu, Teng Wang, Yixiao Ge, Zeyu Lu, Ruisong Zhou, Ying Shan, and Ping Luo. π-tuning: Transferring multimodal foundation models with optimal multi-task interpolation. In *International Conference on Machine Learning*, pp. 37713–37727. PMLR, 2023.

Xun Wu, Shaohan Huang, and Furu Wei. Mixture of LoRA experts. In *International Conference on Learning Representations*, 2024. URL `https://openreview.net/forum?id=uWvKBCYh4S`.

Yichen Wu, Hongming Piao, Long-Kai Huang, Renzhen Wang, Wanhua Li, Hanspeter Pfister, Deyu Meng, Kede Ma, and Ying Wei. Sd-lora: Scalable decoupled low-rank adaptation for class incremental learning. In *The Thirteenth International Conference on Learning Representations*, 2025.

Annie Xie and Chelsea Finn. Lifelong robotic reinforcement learning by retaining experiences. In *Conference on Lifelong Learning Agents*, pp. 838–855. PMLR, 2022.

Mengdi Xu, Yuchen Lu, Yikang Shen, Shun Zhang, Ding Zhao, and Chuang Gan. Hyper-decision transformer for efficient online policy adaptation. In *International Conference on Learning Representations*, 2023. URL `https://openreview.net/forum?id=AatUEvC-Wjv`.

Chuanyu Yang, Kai Yuan, Qiuguo Zhu, Wanming Yu, and Zhibin Li. Multi-expert learning of adaptive legged locomotion. *Science Robotics*, 5(49):eabb2174, 2020.

Enneng Yang, Zhenyi Wang, Li Shen, Shiwei Liu, Guibing Guo, Xingwei Wang, and Dacheng Tao. Adamerging: Adaptive model merging for multi-task learning. In *The Twelfth International Conference on Learning Representations*, 2024.

Zhecheng Yuan, Zhengrong Xue, Bo Yuan, et al. Pre-trained image encoder for generalizable visual reinforcement learning. *Advances in Neural Information Processing Systems*, 35:13022–13037, 2022.

Friedemann Zenke, Ben Poole, and Surya Ganguli. Continual learning through synaptic intelligence. In *International Conference on Machine Learning*, pp. 3987–3995. PMLR, 2017.

Han Zhao, Wenxuan Song, Donglin Wang, Xinyang Tong, Pengxiang Ding, Xuelian Cheng, and Zongyuan Ge. More: Unlocking scalability in reinforcement learning for quadruped vision-language-action models. *arXiv preprint arXiv:2503.08007*, 2025.

Tony Zhao, Vikash Kumar, Sergey Levine, and Chelsea Finn. Learning fine-grained bimanual manipulation with low-cost hardware. *Robotics: Science and Systems XIX*, 2023.

Weixiang Zhao, Shilong Wang, Yulin Hu, Yanyan Zhao, Bing Qin, Xuanyu Zhang, Qing Yang, Dongliang Xu, and Wanxiang Che. SAPT: A shared attention framework for parameter-efficient continual learning of large language models. In *Proceedings of the 62nd Annual Meeting of the Association for Computational Linguistics (Volume 1: Long Papers)*, pp. 11641–11661, 2024.

Dawei Zhou, Hailong Sun, et al. Continual learning with pre-trained models: A survey. *arXiv preprint arXiv:2401.16386*, 2024.

Yuke Zhu, Josiah Wong, Ajay Mandlekar, Roberto Martín-Martín, Abhishek Joshi, Soroush Nasiriany, and Yifeng Zhu. robosuite: A modular simulation framework and benchmark for robot learning. *arXiv preprint arXiv:2009.12293*, 2020.

A Experimental Setup

A.1 Policy and Algorithm Details

Policy Architecture. We use a policy consisting of vision, text, and state encoders, an input modality fusion module, a temporal transformer, and an action head (Liu et al., 2024b;a). We utilize the open-source CLIP ViT/B-16 model (Radford et al., 2021) as vision and text encoders, while all other components of the policy is learned from robot demonstrations. Detailed hyperparameters of each sub-module are summarized in Table 1, most of them are naturally inherited from the open-source LIBERO benchmark and CLIP model.

Baselines. We consider naive sequential fine-tuning baselines, representative lifelong learning methods that involve tuning the entire policy, and several LoRA-based methods:

- Sequential Fine-tuning (SeqFT) (Liu et al., 2024a): Naively perform full fine-tuning (FFT) or use frozen pretrained feature (FPF), i.e., freeze the spatial encoders and fine-tune the rest, on sequentially arriving tasks.
- Experience Replay (ER) (Chaudhry et al., 2019), a *replay* method that maintains a memory buffer with samples from previous tasks. We store a subset of data after each task (20% in our experiments) and uniformly sample a fixed number of replay data from the buffer along with new task data during training. We use a batch size of 32 for old data, consistent with the batch size for new data, and mix them up for every training iteration.
- Elastic Weight Consolidation (EWC) (Kirkpatrick et al., 2017), a *regularization* method that uses the Fisher Information Matrix (FIM) to quantify the importance of each parameter and adds a regularization term to the learning objective to constrain network updates. We set the hyperparameters $\gamma = 0.9$ and $\lambda = 5 \times 10^4$.
- PackNet (Mallya & Lazebnik, 2018), an *architectural* method that first trains and prunes the network to retain a fixed proportion (25% in our experiments) of the most important parameters. The selected parameters are then fine-tuned and frozen to prevent forgetting.
- LifelOng knowledge Transfer Using Skills (LOTUS) (Wan et al., 2024) involves two stages: extracting temporal segment features by leveraging frozen foundation models for skill discovery, and hierarchical imitation learning with the meta-controller and a growing skill library. Since LOTUS employs a distinct architecture, we adjust its parameters to be comparable to our policy and follow the same training pipeline. Additionally, LOTUS utilizes the DINO-v2 (Oquab et al., 2024) foundation model instead of CLIP, as recommended by the ablation study in their paper.
- Task-specific Adapters for Imitation Learning (TAIL) (Liu et al., 2024b) introduces separate LoRAs into the spatial encoder and temporal decoder for each new task. The fusion module, state encoder, and action head are also full fine-tuned and stored as task-specific adapters. TAIL requires an oracle task identifier to retrieve the corresponding adapters during inference. In order to align with other methods, we additionally provide the result of SeqFT (LoRA), which fine-tunes LoRA parameters sequentially.
- Learning to Modulate (L2M) (Schmied et al., 2023) maintains a learnable modulation pool with keys and associated modulators. The embedded history of state tokens serves as the query vector for query-key matching, which finally steers the pretrained policy's behavior. We follow the original paper to use a frozen fusion module and action head, and insert LoRA pools in the CLIP encoders and the temporal transformer backbone. We use a pool size of 30 and the similarity loss coefficient $\lambda = 0.5$.
- Incremental Learning of Retrievable Skills for Continual Imitation Learning (IsCiL) (Lee et al., 2024) establishes multifaceted prototypes through K-means clustering in the state space, where proper LoRA-based skills is retrieved upon current input state. We define the task-specific skill the same as in TAIL (Liu et al., 2024b), i.e., LoRA matrices for transformer, the fusion module, the state

Table 1: Policy Configurations

Hyperparameter	Value
Vision & Text Encoder	
Pretrained model	CLIP ViT-B/16
Image resolution	128*128
Proprioceptive States	
Joint state dim.	7
Gripper state dim.	2
Modality Fusion	
Number of hidden layers	1
Hidden size	256
Activation	GELU
Temporal Transformer	
Number of layers	6
Number of attn. heads	8
Embedding size	768
MLP hidden size	1024
Max sequence Length	10
Dropout	0.15
Action Head	
Number of hidden layers	2
Hidden size	256
Number of Modes	5
Min. std	1e-4
Activation	Softplus
Action dim.	7
Expert router	
Number of hidden layers	2
Hidden Activation	GELU
Output Activation	Sigmoid

Table 2: Training Hyperparameters

Hyperparameter	Value
Optimizer	
Training epochs	10
Batch size	32
Optimizer	AdamW
Betas	(0.9,0.999)
Learning rate	1e-4
Anneal strategy	cos
Weight decay	0.1
Gradient clip	100
Image Augmentation	
Brightness	0.3
Saturation	0.3
Contrast	0.3
Hue	0.3
Color jitter prob.	0.9
Rotation	15
Translation	0.1
Affine prob.	0.6
Evaluation	
Epochs per eval.	2
Eval. episodes	20

encoder, and the action head. We use CLIP encoded features as context embeddings and set the skill prototype $\mathcal{X}_z$ in $\mathcal{X}$ to be composed of 20 bases.

We utilize the implementations of SeqFT, ER, EWC, and PackNet provided in LIBERO (Liu et al., 2024a) and we directly use the official code of LOTUS (Wan et al., 2024). When training with ER and EWC, we use two GPUs, each with a batch size of 16, ensuring the total batch size remains consistent with other methods. Due to the unavailability of publicly released code for TAIL, we implemented it based on the description in the paper (Liu et al., 2024b). We integrated the code for L2M and IsCiL into our codebase, as the original implementations operate with different policies in different benchmarks.

For LoRA-based methods, we insert LoRA modules with rank $r = 8$ into the 6-th to 11-th layers of the CLIP image and text encoders, and LoRA modules with $r = 16$ into the temporal transformer. LoRA is applied to the query and value projection matrices. In TAIL and IsCiL, we learn task-specific fusion modules, state encoders, and action heads, as described in (Liu et al., 2024b). In contrast, these components are frozen in L2M following the original paper (Schmied et al., 2023).

DMPEL (Ours). We adopt the same settings in the image encoder, text encoder, and temporal transformer as other LoRA-based methods, and use LoRA experts with $r = 16$ for all linear layers in other sub-modules. Besides, in the Long suite, we tune both the low-rank weights $\boldsymbol{A}, \boldsymbol{B}$ and biases $\boldsymbol{b}$, whereas in the Goal, Spatial, and Object suites, we only tune the low-rank weights $\boldsymbol{A}, \boldsymbol{B}$. However, both settings lead to fewer learnable

Algorithm 2 Inference Process of DMPEL

Require: Pretrained policy π_θ, router $\mathcal{R}$, each layer with pretrained weight and low-rank expert library $\{\mathcal{F}, \mathcal{L}\}$, FIFO queues $F_q = \varnothing$, $R_q = \varnothing$ with maximum length T

for $t = 1, 2, \cdots, \mathcal{H}$ **do**
  Observe $o_t = (I_t^1, \cdots, I_t^{N_c}, p_t)$ and language instruction l
  if $T_{\text{syn}} \mid t$ **then**
    Compute visual and textual embeddings $\tilde{f}_t^v$, $\tilde{f}_t^l$ using the frozen CLIP encoders $\mathcal{E}_I$, $\mathcal{E}_L$ ($\mathcal{F}$ only)
    Compute the context embedding $\boldsymbol{r}_t = [\tilde{f}_t^v, \tilde{f}_t^l, p_t]$
    $R_q \leftarrow R_q \cup \{\boldsymbol{r}_t\}$
    Compute the expert coefficient vector $\boldsymbol{c}_t = \text{top-}k(\mathcal{R}(\boldsymbol{r}_{t-T:t}))$
    for each $\{\mathcal{F}, \mathcal{L}\}$ **do**
      Obtain the expert coefficient $\boldsymbol{c}_t^\diamond$ according to which sub-module $\diamond$ the layer belongs to
      Synthesize parameters $\tilde{\boldsymbol{W}}, \tilde{\boldsymbol{b}}$ using Eq. (7)
    end for
  else
    Reuse previous visual and text embeddings $\tilde{f}_t^v \leftarrow \tilde{f}_{t-1}^v$, $\tilde{f}_t^l \leftarrow \tilde{f}_{t-1}^l$
    $R_q \leftarrow R_q \cup \{[\tilde{f}_t^v, \tilde{f}_t^l, p_t]\}$
  end if
  Compute visual, textual, and state embeddings f_t^v, f_t^l, f_t^s using encoders $\mathcal{E}_I$, $\mathcal{E}_L$, $\mathcal{E}_P$ ($\mathcal{F}$ and $\mathcal{L}$)
  Obtain $f_t \in \mathbb{R}^{\text{num of modalities} \times \text{embedding dim}}$ using FiLM to fuse language embeddings with image and state embeddings
  $F_q \leftarrow F_q \cup \{f_t\}$
  Compute latent embedding $g_t = \mathcal{D}_T(f_{t-T}, \cdots, f_{t-1}, f_t)$
  Predict action $a_t = \mathcal{D}_H(g_t)$
  Interact with the environment using action a_t and obtain done flag d_{t+1}
  if d_{t+1} is True **then break**
end for

parameters than TAIL (Liu et al., 2024b), which learns these sub-modules separately for each task. We also employ dropout with probability $p = 0.15$ on the coefficient for low-rank experts to avoid overfitting.

A.2 Training Configuration

We generally follow the setup in the LIBERO benchmark for training and evaluation (Liu et al., 2024a). For all experiments, we use either Nvidia A100 or H800 GPUs. We employ Distributed Data Parallel (DDP) for parallel training across 4 GPUs during pretraining, while using a single GPU for lifelong learning. We employ 16-bit floating point precision (FP16) for training and inference to accelerate the process, with the exception of the router, which uses FP32. This selective precision technique is also discussed in (Fedus et al., 2022). To ensure reproducibility and statistical significance, we adopted three random seeds (100, 200, 300) and reported the mean and standard deviation of the performance over three seeds throughout the paper.

We deviate from the original LIBERO benchmark by training each task for only 10 epochs (evaluate every 2 epochs), instead of 50 epochs (evaluate every 10 epochs), as we observed convergence typically within 10 epochs. Consequently, metrics including FWT and AUC that are averaged over epochs generally appear lower than those reported in the original LIBERO paper and some follow-up work. We also explored various hyperparameter settings for DMPEL, such as top-k selection, replay ratio coefficients, and weight initialization; these ablations are detailed in Figure 5. Otherwise, we use the same training hyperparameters across all methods and benchmarks, which proved effective. Hyperparameter details are summarized in Table 2.

A.3 Benchmark Details

We present the specific language instructions for the tasks in four lifelong learning LIBERO task suites in Table 3. Although some tasks have similar descriptions, they are not identical due to differences in

Table 3: Tasks Instructions of LIBERO Task Suites

Benchmark Suite	Task Instructions
LIBERO-Goal	open the middle drawer of the cabinet put the bowl on the stove put the wine bottle on top of the cabinet open the top drawer and put the bowl inside put the bowl on top of the cabinet push the plate to the front of the stove put the cream cheese in the bowl turn on the stove put the bowl on the plate put the wine bottle on the rack
LIBERO-Spatial	pick up the black bowl between the plate and the ramekin and place it on the plate pick up the black bowl next to the ramekin and place it on the plate pick up the black bowl from table center and place it on the plate pick up the black bowl on the cookie box and place it on the plate pick up the black bowl in the top drawer of the wooden cabinet and place it on the plate pick up the black bowl on the ramekin and place it on the plate pick up the black bowl next to the cookie box and place it on the plate pick up the black bowl on the stove and place it on the plate pick up the black bowl next to the plate and place it on the plate pick up the black bowl on the wooden cabinet and place it on the plate
LIBERO-Object	pick up the alphabet soup and place it in the basket pick up the cream cheese and place it in the basket pick up the salad dressing and place it in the basket pick up the bbq sauce and place it in the basket pick up the ketchup and place it in the basket pick up the tomato sauce and place it in the basket pick up the butter and place it in the basket pick up the milk and place it in the basket pick up the chocolate pudding and place it in the basket pick up the orange juice and place it in the basket
LIBERO-Long	put both the alphabet soup and the tomato sauce in the basket put both the cream cheese box and the butter in the basket turn on the stove and put the moka pot on it put the black bowl in the bottom drawer of the cabinet and close it put the white mug on the left plate and put the yellow and white mug on the right plate pick up the book and place it in the back compartment of the caddy put the white mug on the plate and put the chocolate pudding to the right of the plate put both the alphabet soup and the cream cheese box in the basket put both moka pots on the stove put the yellow and white mug in the microwave and close it

environment configurations, such as varying spatial layouts, objects, or goal positions. Each task provides 50 successful expert demonstrations for imitation learning.

B Additional Results

B.1 Ablation Studies

Task Order. We further investigate the performance of DMPEL across various settings. First, we assess its robustness to different task orders, as shown in Figure 9a. The default order provided by the LIBERO benchmark is 0123456789, the reverse order is 9876543210, and the randomly generated task order is 4687312095.

Rank Size. We analyze the impact of the rank size of each LoRA expert in Figures 9b. Performance generally improves as the rank size increases, but shows saturation at a rank size of 32, indicating a trade-off between parameter efficiency and performance. Additionally, we compare the lifelong PEFT baselines (TAIL, IsCiL, and DMPEL) under the same total number of LoRA experts. Notably, DMPEL with top-3 activation activates three LoRA experts simultaneously, while the others activate only one. Therefore, we present the results for TAIL and IsCiL with the rank increased by three times in Table 4. However, the results show that naively increasing the rank size for the baselines does not achieve the same performance as DMPEL, highlighting the effectiveness of using a LoRA expert library with expert coefficient replay.

Number of Demos. We illustrate the impact of the number of demonstrations for each new task in Figure 9c. The performance of FWT remains quite stable when the number of demonstrations ranges from 10 to 50, indicating that DMPEL can effectively adapt across tasks even in low-data regimes.

Router Design. We utilize the Sigmoid function to constrain the router output instead of applying Softmax normalization. As noted in the related work, DMPEL is heavily inspired by research on model fusion and merging, such as SD-LoRA (Wu et al., 2025) and LoRAHub (Huang et al., 2024), which demonstrate that adjusting only the magnitude of LoRA can yield promising transfer results. The interval [0, 2] serves as a hyperparameter based on intuition to limit the magnitude, with 1 as the midpoint, representing the direct use of the previous LoRA module without magnitude alteration. We empirically compare the performance of Sigmoid and Softmax with various top-k strategies, as shown in Figure 10. Notably, router with Sigmoid generally outperforms the ones with Softmax, and the top-1 with Softmax variant exhibited the lowest performance. We hypothesize that using raw coefficients to modulate the magnitudes of LoRA experts provides greater flexibility, as these coefficients are independent for each expert. In contrast, Softmax normalization enforces that the sum of coefficients equals 1, meaning that increasing one coefficient necessarily decreases another. During expert coefficient replay, we apply the MSE loss between old and new coefficients in all cases for its simplicity. When transitioning from task K to task $K+1$, we pad the coefficient vector with 0 to maintain alignment with the current library size and ensure that later introduced experts are excluded from previous tasks. We hypothesize that minimizing the discrepancy of logits may be a more effective approach for the top-1 Softmax variant due to its one-hot property. In this context, padding zeros to the coefficients becomes padding $-\infty$ to the logits. We leave further investigation of this for future work.

Top-k Mismatch between Training and Evaluation. We present the performance of DMPEL with a differing number of top-k LoRA experts between training and evaluation in Table 5. Although there is only a slight decrease in success rate (e.g., 2%), this allows for adaptive scaling based on computational

Table 4: Performance on LIBERO-Goal with Different Rank Size

Method	Rank Size	FWT	BWT	AUC
TAIL (with task ID)	rank	0.54 ± 0.03	0	0.67 ± 0.06
TAIL (with task ID)	rank × 3	0.55 ± 0.03	0	0.71 ± 0.02
ISCiL	rank	0.54 ± 0.04	0.05 ± 0.03	0.60 ± 0.06
ISCiL	rank × 3	0.52 ± 0.02	0.09 ± 0.06	0.59 ± 0.05
DMPEL w/ top-1	rank	0.61 ± 0.03	0.01 ± 0.02	0.68 ± 0.03
DMPEL w/ top-3	rank	0.68 ± 0.03	0.00 ± 0.01	0.78 ± 0.02

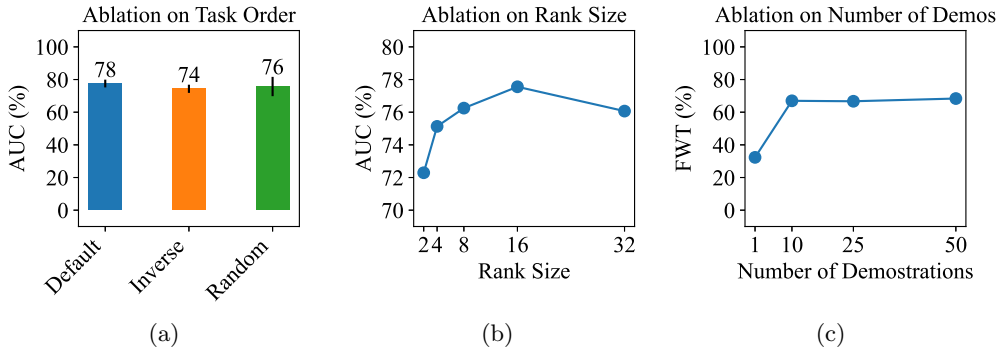

Figure 9: Ablation studies in the LIBERO-Goal suite. (a) Different task orders (b) Different rank sizes (c) Different number of demonstrations.

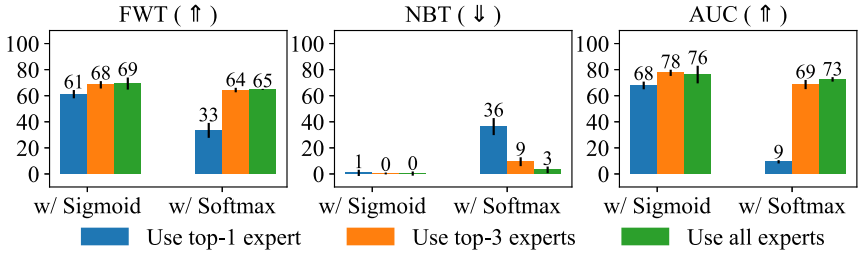

Figure 10: Ablation studies on router design in the LIBERO-Goal suite.

resource constraints. Furthermore, training with multiple experts while using the top-1 expert yields better performance than training with only the top-1 expert, likely due to enhanced robustness during training.

B.2 Pretrained Policy with PEFT vs Separate Policy

The *pretrain-then-finetune* paradigm has proven to be highly successful in the domains of vision, language, and robotics. It is widely believed that pretrained models capture common knowledge that can be leveraged for various downstream tasks, enabling rapid transfer or even zero-shot transfer. Meanwhile, *parameter-efficient fine-tuning* (PEFT) techniques have shown great effectiveness in steering frozen foundation models by incorporating small, learnable modules during adaptation. Therefore, the results presented in the main text are based on a setting where a large policy is first pretrained on the LIBERO-90 dataset before being transferred to streaming tasks. We also demonstrate the performance gains achieved by pretraining compared to starting from scratch. To further illustrate effectiveness, we compare our approach with training separate models for each individual task in Table 6. We present results using the policy ViT-T provided in the original LIBERO benchmark with two different sizes: the smaller model has 1.9M parameters (similar to that of a LoRA expert), while the larger model has 17.7M parameters (the total number of all models after 10 tasks will be comparable to that of the single large policy used in the main experiment). The results reveal a significant gap between using dedicated small models and employing a single large pretrained policy enhanced with LoRA experts, underscoring the effectiveness of DMPEL.

Table 5: Performance on LIBERO-Goal with Different Top-k Experts Used in Training and Evaluation

Training	Evaluation	Average Success Rate
Use all experts	Use all experts	0.79 ± 0.06
Use all experts	Use top-3 experts	0.81 ± 0.05
Use all experts	Use top-1 experts	0.77 ± 0.05
Use top-3 experts	Use top-3 experts	0.81 ± 0.05
Use top-3 experts	Use top-1 experts	0.79 ± 0.01
Use top-1 expert	Use top-1 expert	0.69 ± 0.05

B.3 Visualization Analysis

LoRA Expert Activation Trajectories. We plot representative trajectories from different benchmark suites in Figures 14-15, with labels indicating the expert ID from the library. In Figure 14, we observe that the policy relies on the newly introduced expert 2 when executing task 2. In task 9 that also involves picking up a bowl but placing it down at a different destination, the vision encoder consistently activates expert 2 throughout the trajectory, while the temporal decoder primarily reuses expert 2 during the first half of the trajectory, likely due to a similar action pattern. Similarly, in Figure 15, the vision encoder reuses previously learned expert but the fusion sub-module learns a new expert to effectively fuse features for manipulation.

LoRA Expert Similarities across Tasks. We also examine the cosine similarity between experts $\boldsymbol{A}_K\boldsymbol{B}_K$ taken from the final block of the image encoder and the temporal transformer. The results in Figure 12 highlight the key difference between TAIL and DMPEL. TAIL sequentially fine-tunes a single LoRA expert and stores a copy at the end of each task for future retrieval, hence the similarities between experts are high, especially those from adjacent tasks. In contrast, DMPEL initializes each newly introduced LoRA expert orthogonally, and the active LoRA expert is always a dynamic mixture of these orthogonal experts drawn from the library.

Correlation between Context Embedding Similarity and Expert Activation Coefficient Similarity. Since the LoRA expert activation coefficients are generated conditioned on the current observation context, similar context embeddings should intuitively lead to similar expert activations. Figure 13 shows a hexagonal binning plot of the relationship between pairwise cosine similarity of task embeddings and pairwise cosine similarity of expert activations. The Pearson correlation coefficient is approximately 0.46, indicating a clear positive relationship.

Action Space Coverage. In Section 5.2 Figure 6, we empirically observe that the low-rank expert learned for the action head in the first task is extensively reused in subsequent tasks, while the experts introduced later are rarely activated. The LIBERO benchmark is built on the Robosuite framework (Zhu et al., 2020), where the default underlying controller is OSC_POSE (Operational Space Control with Pose). The action includes the 6D end-effector (EEF) poses (position & orientation) and the status of gripper, $a = [\mathrm{d}x, \mathrm{d}y, \mathrm{d}z, \mathrm{d}\alpha, \mathrm{d}\beta, \mathrm{d}\gamma, \mathit{gripper}]$. Seven dimensions respectively corresponds to translation along the x-axis, y-axis, and z-axis, the roll (α), pitch (β), and yaw (γ) rotation, along with the open/close status of the gripper. We visualize ten action trajectories from the LIBERO-Object benchmark in Figure 11, illustrating that coverage of the action space varies from task to task. Prior research has demonstrated that using different action spaces (e.g., position control vs. velocity control) can significantly affect control performance (Zhao et al., 2023; Chi et al., 2025), and we intend to explore this further in future work.

B.4 Ultra-long Task Sequence

Beyond the experiment on the standard $K = 10$ task sequence form the LIBERO benchmark, we also investigate the applicability of DMPEL to ultra-long sequences. To this end, we concatenate the LIBERO-Object, Goal, and Spatial benchmark to form a task sequence with $K = 30$. Following the empirical analysis in Section 5.2 and illustrated in Figure 6b, we prune underactivated low-rank experts every 10 tasks to control the linear growth of the library. At the end of the 30-th task, as shown in Table 7, the number of LoRA experts in each module (the elements of the six-dimensional vector in order representing the vision encoder, text encoder, state encoder, modality fusion module, temporal transformer, and action head) typically remains

Table 6: Performance on LIBERO-Goal with a Separate Policy for each Individual Task

Method	Number of Parameters	FWT	BWT	AUC
ViT-T (Small)	1.9M (×10)	0.04 ± 0.01	0	0.08 ± 0.01
ViT-T (Large)	17.7M (×10)	0.21 ± 0.04	0	0.43 ± 0.04
DMPEL	174.1M + 1.2M (×10)	0.68 ± 0.03	0.00 ± 0.01	0.78 ± 0.02

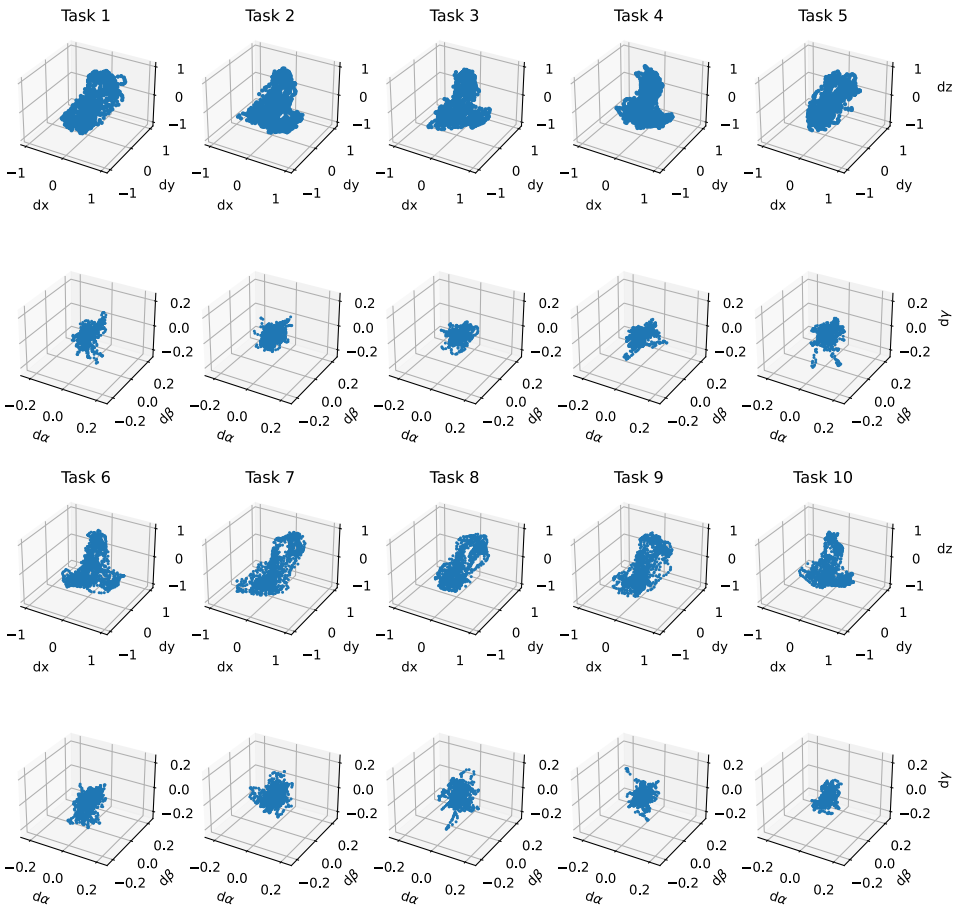

Figure 11: Visualization of the action trajectories from demonstrations of LIBERO-Object benchmark.

below 30, resulting in a compact library that exhibits effective knowledge sharing. The results shown in Figure 16 and Table 7 indicate that DMPEL consistently outperforms FFT with experience replay in success rate, while incurring significantly lower computational and storage costs. However, we still observe a gradual decline in performance as the number of tasks increases. Given the small size of the router, this is not surprising. When the number of distinct tasks continue to increase, the plasticity of the router may be exhausted. We further use a router that is twice as deep and twice as wide (i.e., 2× the number of hidden layers and 2× the hidden dimension) compared to the one in the main experiment. Results in Figure 16 show that DMPEL with the larger router achieves performance comparable to the original model, with a slight advantage after task 20. A more systematic exploration of larger routers and more advanced router architectures is left for future work. We also provide the per-task success rates for tasks 2, 5, 8, 13, 15, and 18 over the entire lifelong learning process in Figure 17. Results show that DMPEL indeed exhibits significant

Table 7: Storage and Computational Cost at the End of an Ultra-long Task Sequence ($K = 30$)

Method	**Number of LoRA Experts and Parameters in Each Module**	**Trainable Parameters**	**Additional Storage for Replay**
DMPEL	[15,18,17,21,17,10], 10.7M (seed=100) [18,19,17,19,17,7], 11.1M (seed=200) [20,18,20,19,18,9], 11.7M (seed=300)	1.2M	0.06GB
ER	/	174.1M	3.7GB

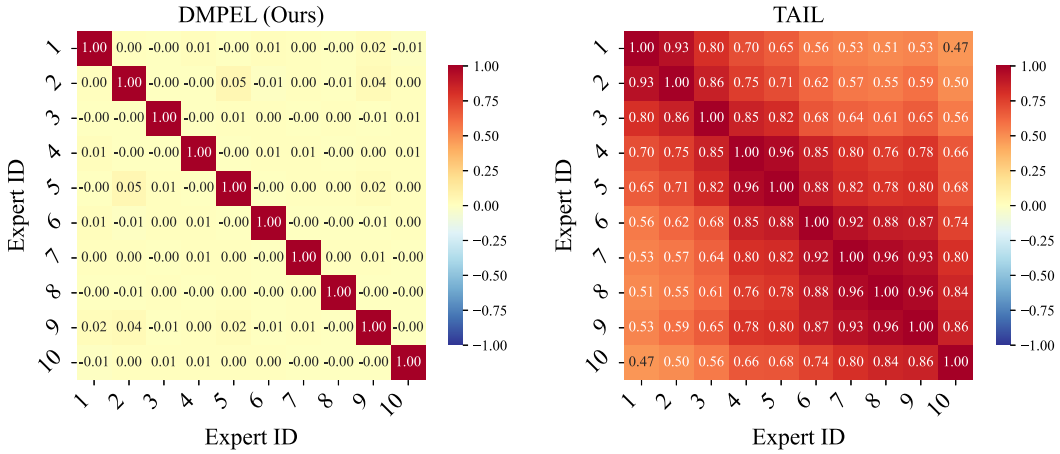

(a) The query projection matrix of the final block in image encoder

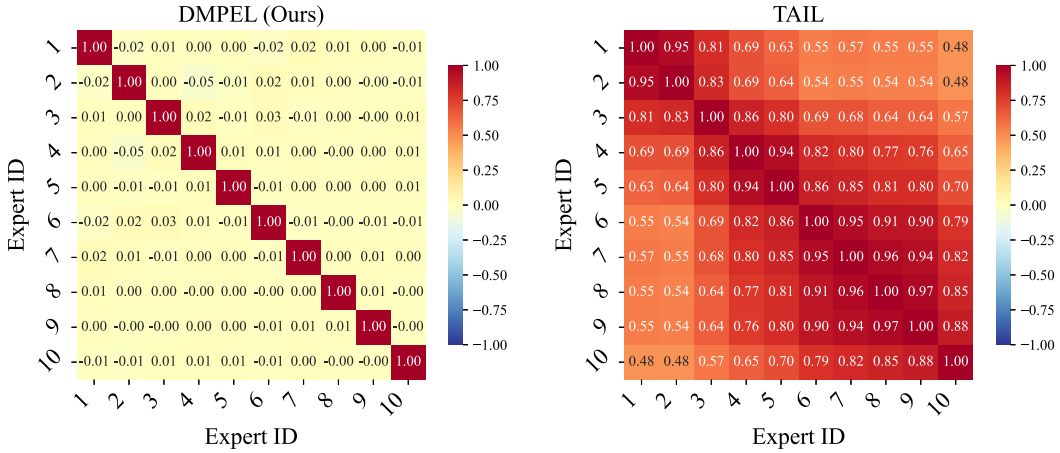

(b) The query projection matrix of the final block in temporal transformer

Figure 12: Visualization Analysis on LoRA Expert Similarities across Tasks.

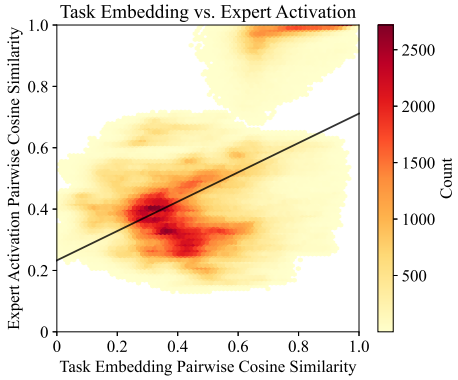

Figure 13: Visualization of the action trajectories from demonstrations of LIBERO-Object benchmark.

long-term resistance to forgetting. Besides, for some tasks (e.g., Task 2 and 5), the router size has little impact on forgetting, whereas for others (e.g., Tasks 8 and 15), a larger router exhibits better.

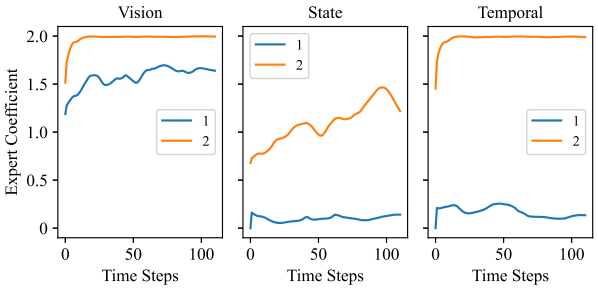

(a) Trajectory of expert coefficient $\boldsymbol{c}$

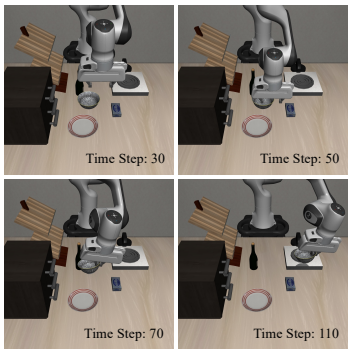

(b) Side-view image

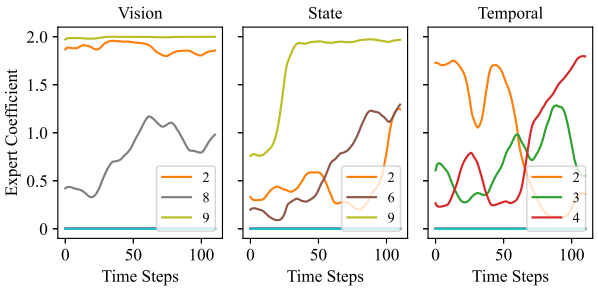

(c) Trajectory of expert coefficient $\boldsymbol{c}$

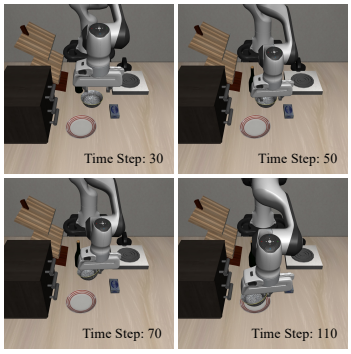

(d) Side-view image

Figure 14: Visualization Analysis on Expert Activation: (a)-(b) Task 2 from LIBERO-Goal: put the bowl on the stove; (c)-(d) Task 9 from LIBERO-Goal: put the bowl on the plate.

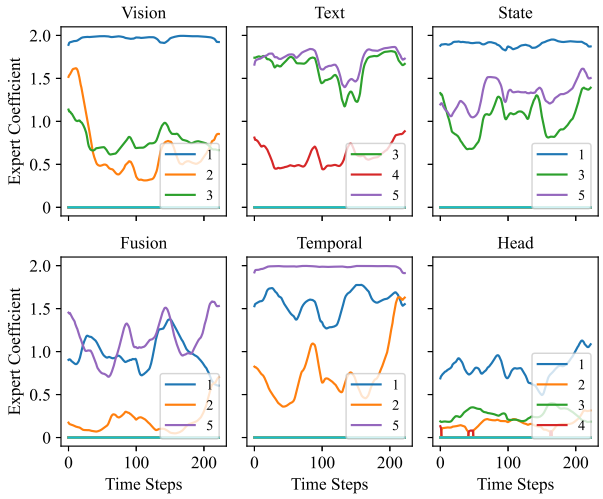

(a) Trajectory of expert coefficient $\boldsymbol{c}$

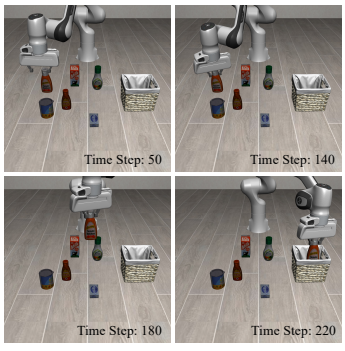

(b) Side-view image

Figure 15: Visualization Analysis on Expert Activation: Task 5 from LIBERO-Object: pick up the ketchup and place it in the basket.

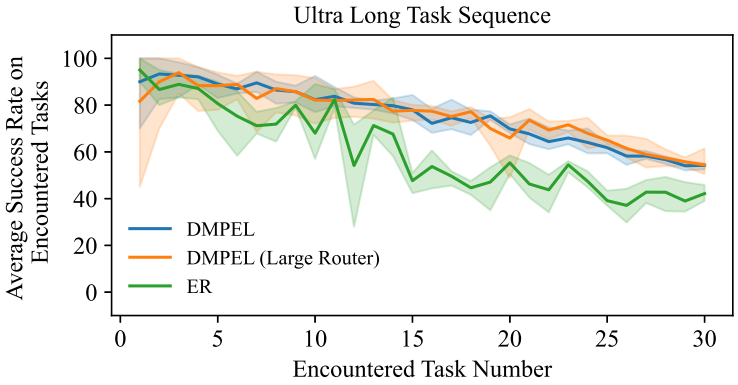

Figure 16: Average success rate on encountered tasks in the ultra long task sequence concatenated with LIBERO-Object, Goal, and Spatial benchmarks.

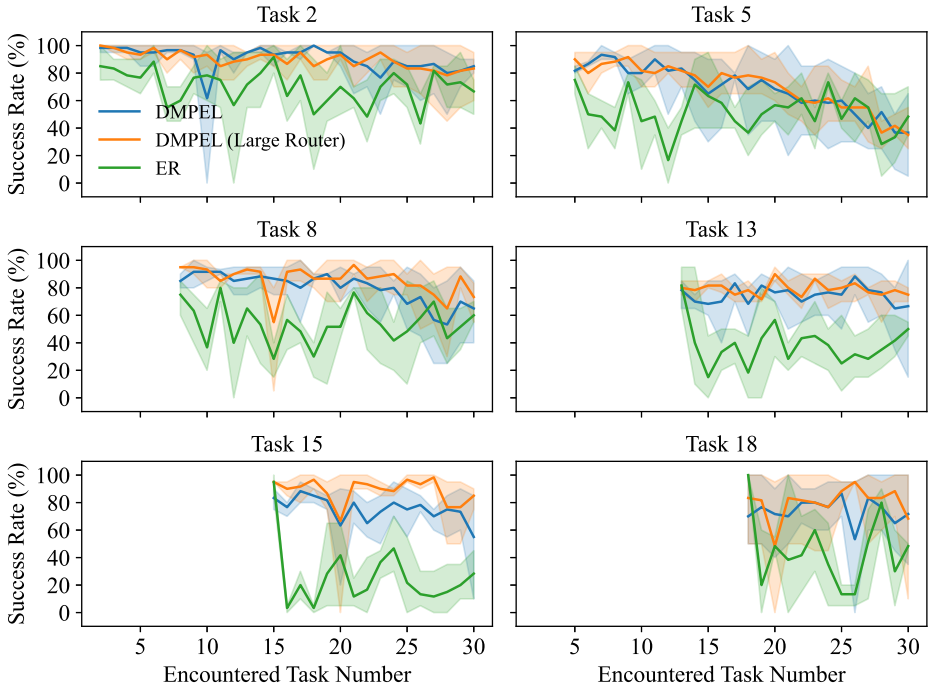

Figure 17: Success rate on task 2, 5, 8, 13, 15, 18 in the ultra long task sequence.

B.5 Cross-domain Adaptation

While LIBERO is a large-scale multi-modal benchmark that requires complex behavior and hence giving promising results, we further evaluate the cross-domain adaptation capabilities of DMPEL. We conduct experiments with the same hyperparameters on three tasks (Lift, Can, and Square) from Robomimic (Mandlekar et al., 2022), which together form a task sequence with $\kappa = 3$. These tasks share the same observation and action space, but feature novel backgrounds and objects. The results in Table 8 demonstrate that DMPEL can be effectively applied to lifelong adaptation in the Robomimic benchmark, achieving better performance than IsCiL and a similar AUC to TAIL which uses oracle task IDs.

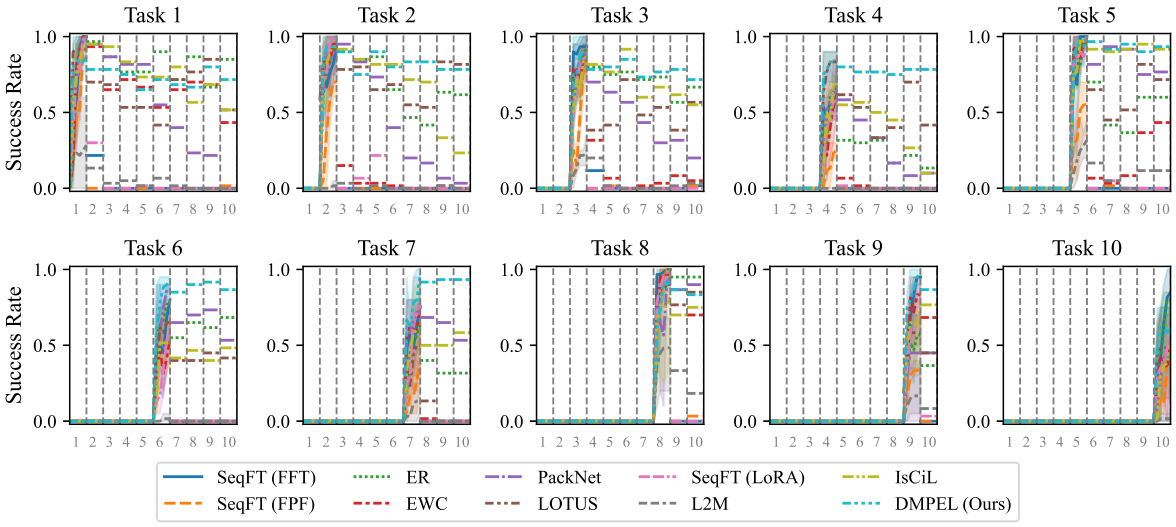

Figure 18: Visualization of learning curves on the LIBERO-Goal benchmark.

B.6 Learning Curves

We present the learning curves for all methods in four lifelong learning LIBERO task suites in Figure 18-21 . The y-axis indicates the success rate, while the x-axis depicts the agent's training process over the course of lifelong learning. For example, the Task 1 subplot in the figure shows the agent's performance on the first task when it learns ten tasks sequentially. Learning curves demonstrate that DMPEL achieves superior forward transfer with reduced forgetting compared to baselines.

C Discussions and Future Directions

C.1 Scaling to Larger Model and Longer Task Sequences.

We conducted pretraining and adaptation experiments with a transformer-based model with around 200M parameters, and use a task sequence with up to 30 distinct tasks. Future work can explore scaling up to larger models and longer sequence: (1) Additional computational and storage cost of the expert library. During inference we merging the parameters of the top-k experts to synthesize $\tilde{\boldsymbol{W}} \in \mathbb{R}^{d_{\text{in}} \times d_{\text{out}}}$, which incurs approximately $2 \times k \times r \times (d_{\text{in}} + d_{\text{out}})$ FLOPs. Given the sparse activation of experts (where k is a constant), the computational cost remains stable throughout the lifelong learning process and is significantly lower than that of the forward pass through the pretrained linear layer, which requires $2 \times d_{\text{in}} \times d_{\text{out}}$ FLOPs (noting that $r \ll d_{\text{in}}, d_{\text{out}}$). Consequently, regardless of the task sequence length or policy size, the additional computation remains a fixed proportion relative to the pretrained backbone, which is $\frac{kr(d_{\text{in}}+d_{\text{out}})}{d_{\text{in}}d_{\text{out}}}$. For instance, when $d_{\text{in}} = d_{\text{out}} = 768$, $r = 8$, $k = 3$, then the additional proportion is 6.3%. (2) Additional storage overhead introduced by the coefficient replay mechanism. As introduced in Section 4.3, we archive a subset of the router's input–output pairs for future replay, namely the context embedding $\boldsymbol{r}$ and the coefficient vector $\boldsymbol{c}$. In our main experiments, the embedding dimension is 768, following the CLIP model, while the dimension

Table 8: Performance on cross-domain lifelong adaptation to Robomimic ($K = 3$)

Method	FWT	BWT	AUC
DMPEL	0.54 ± 0.05	0.10 ± 0.02	0.54 ± 0.02
IsCiL	0.46 ± 0.05	0.14 ± 0.06	0.48 ± 0.04
SeqFT (LoRA)	0.42 ± 0.01	0.49 ± 0.02	0.26 ± 0.05
TAIL (w/ task ID)	0.42 ± 0.01	0	0.54 ± 0.05

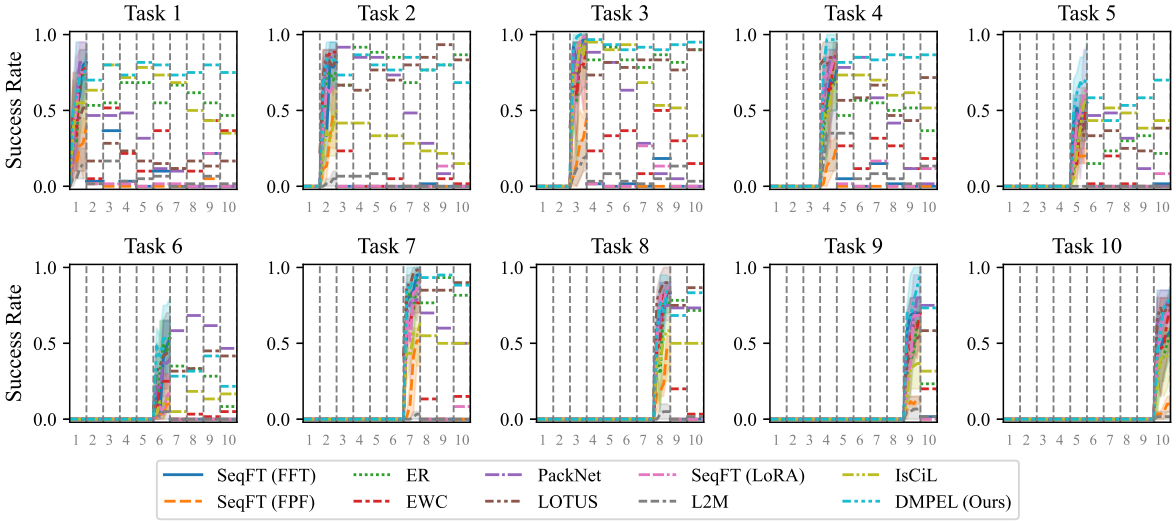

Figure 19: Visualization of learning curves on the LIBERO-Spatial benchmark.

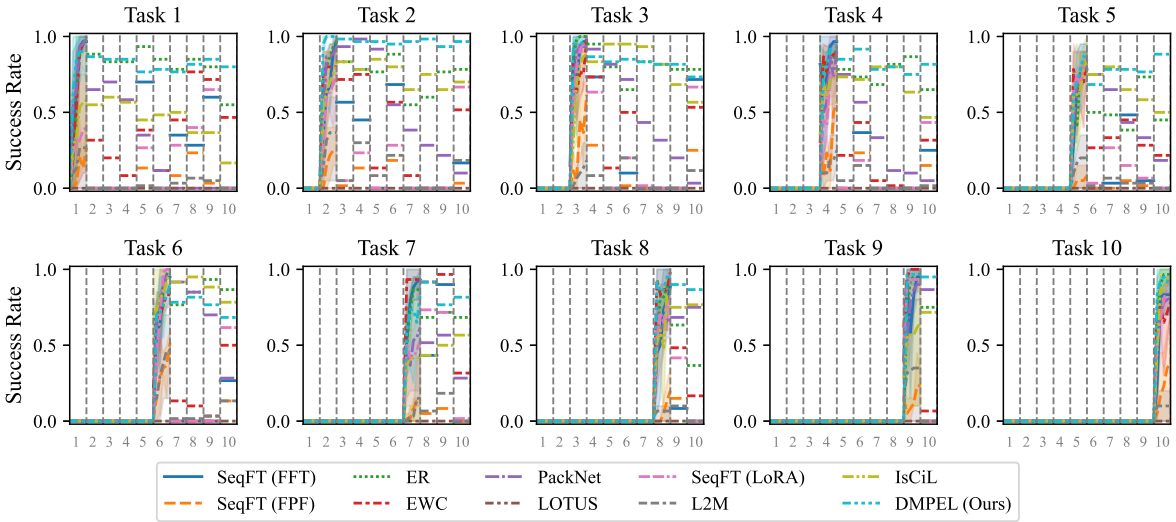

Figure 20: Visualization of learning curves on the LIBERO-Object benchmark.

of the coefficient vector grows with the size of the expert library and is typically less than 100. When scaling to larger models, the embedding dimension increases, but modern LLMs/VLMs usually use 4k–8k embedding dimensions for 10B–100B parameter models. When scaling to ten-times-longer task sequences where $\kappa > 100$, we expect the dimension of the coefficient vector to increase by up to a factor of ten if the number of submodules remains fixed. Therefore, the overall storage overhead remains tractable. (3) Capacity and plasticity of the router in long task sequences. The expert router in DMPEL maps context embeddings to activation coefficients for each LoRA expert in the library. Consequently, we do not predefine a fixed number of tasks; instead, the expert library, the router, and the coefficient replay buffer are all dynamically expanded. Note that we only increase the output dimension of the router's final linear layer to keep them aligned. Therefore, as the number of distinct tasks continues to grow, a potential way to maintain the MLP's plasticity is to progressively scale up the router as well. For example, increasing the number of hidden layers and the hidden-layer width so that the context can be projected into a higher-dimensional space and more essential information can be captured. Since we store all expert coefficients in the replay buffer during lifelong adaptation, we should be able to recover the coefficient distribution with the enlarged new router. We leave a systematic exploration of this direction to future work.

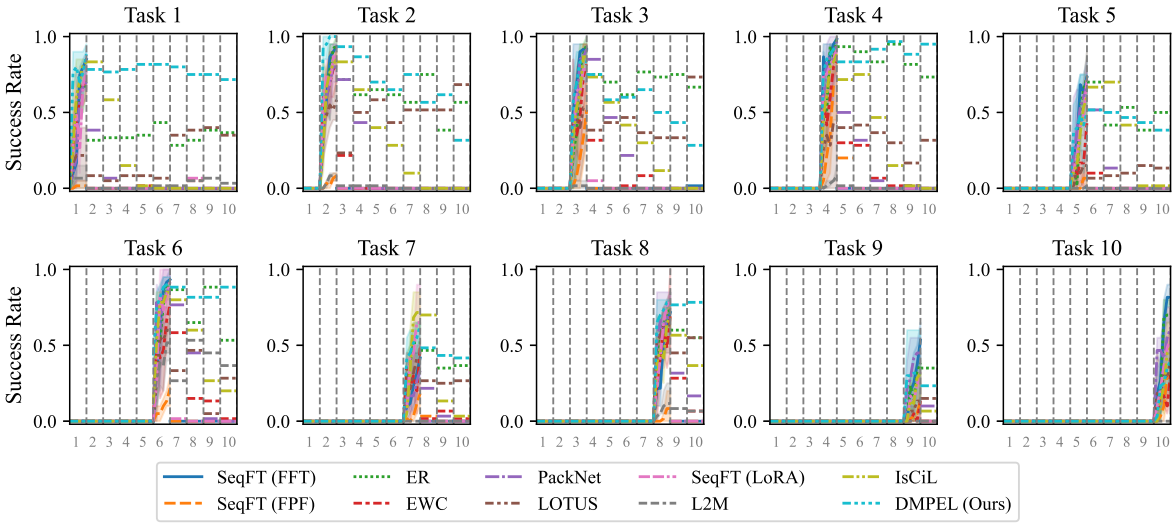

Figure 21: Visualization of learning curves on the LIBERO-Long benchmark.

C.2 Sim2Real Transfer.

Future work can focus on addressing the following challenges for sim2real transfer: (1) Differences in visual input. There are substantial discrepancies between images produced by simulation engines and those captured by real-world sensors, which necessitates further fine-tuning of the visual encoder; (2) Differences between simulated and real robots. Even when using the same robot (e.g., the Franka Emika Panda), minor differences can lead to varying end-effector behaviors, underscoring the necessity of demonstrations collected on the actual robot; (3) Real-world stochasticity. The unpredictability of real-world environments adds complexity to the transfer process. One potential solution is to incorporate a post-fine-tuning step for the pretrained policy using real-world datasets before initiating lifelong adaptation in the real environment. Given DMPEL's performance in the large-scale simulated benchmark LIBERO, we expect it to perform well during the lifelong adaptation phase. However, we would like to emphasize that the sim2real domain has a wealth of related work that is generally orthogonal to lifelong learning approaches and could be promising research directions.